

UNIVERSITY OF ILLINOIS

May 13 1987

THIS IS TO CERTIFY THAT THE THESES PREPARED UNDER MY SUPERVISION BY

Brian Grady

ENTITLED Flow-Induced Crystallization of

PVE₂

IS APPROVED BY ME AS FULFILLING THIS PART OF THE REQUIREMENTS FOR THE

DEGREE OF Bachelor of Science

AJ McHugh

Instructor in Charge

APPROVED J. H. Kostwater for R. C. Moore

HEAD OF DEPARTMENT OF Chemical Engineering

FLOW-INDUCED CRYSTALLIZATION OF
POLYVINYLIDENE FLUORIDE

BY

BRIAN P. GRADY

THESIS

for the

DEGREE OF BACHELOR OF SCIENCE

IN

LIBERAL ARTS AND SCIENCES

College of Liberal Arts and Sciences

University of Illinois

Urbana, Illinois

1987

TABLE OF CONTENTS

List of Figures	i
Acknowledgements	iii
I Introduction	1
II Background	
A. Flow-Induced Crystallization	
1) Formation	3
2) Morphology and Molecular Weight Fractionation	19
B. Polyvinylidene Fluoride	24
III Experimental	
A. Materials	32
B. Fiber growth experiments	32
C. Shear-thickening experiments	33
D. DSC and Optical Microscopy	38
IV Results and Discussion	
A) Fiber growth experiments	39
B) Optical Microscopy	44
C) DSC	49
D) Shear-thickening experiments	52
V Conclusions and Recommendations	58
VI References	60
Appendix A: Computer program used to process shear-thickening experiments	

LIST OF FIGURES

Figure 1:	Illustration showing secondary flow pattern arising in a Couette geometry.....	5
Figure 2:	Illustration of impinging jet geometry used in fiber growth experiments.....	7
Figure 3:	Illustration of surface-growth apparatus used in fiber growth experiments.....	9
Figure 4:	Illustration of model used in Mackley's analysis to show that elongational flow occurs at the tip of the seed crystal in fiber growth experiments.....	11
Figure 5:	Illustration of tubular-growth apparatus used in fiber growth experiments.....	12
Figure 6:	Illustration of tail-train loop model used to explain how adsorbed polymer provides the nucleation necessary for fiber growth.....	15
Figure 7:	Illustration of the transformation from entanglements to fibers.....	17
Figure 8:	Graph showing typical shear thickening behavior. (UHMWPE in xylene, concentration=0.005%).....	18
Figure 9:	Illustration showing shish-kebab morphology.....	20
Figure 10:	Electron micrograph of polyethylene fibers grown from a 5% solution in xylene at 104.8°C.....	21
Figure 11:	Illustration showing molecular backbone and unit cell for the alpha phase of PVF ₂	26
Figure 12:	Illustration showing molecular backbone and unit cell for the beta phase of PVF ₂	28

Figure 13:	Diagram showing the polymorphic transitions of PVF ₂	30
Figure 14:	Illustration showing Couette apparatus used in fiber growth experiments.....	33
Figure 15:	Illustration of Ubbelohde viscometer used in shear-thickening experiments.....	35
Figure 16:	Illustration of overall viscometry set-up used in shear-thickening experiments.....	36
Figure 17:	Photomicrographs of washed PVF ₂ fibers magnified 400x.....	45
Figure 18:	Photomicrograph of washed PVF ₂ fibers magnified 40x.....	47
Figure 19:	Photomicrograph of unwashed PVF ₂ fibers magnified 40x.....	48
Figure 20:	DSC of untreated PVF ₂	50
Figure 21:	DSC of unwashed PVF ₂ fibers.....	51
Figure 22:	DSC of washed PVF ₂ fibers.....	53
Figure 23:	Graph showing shear-thickening behavior of PVF ₂ for T=95°C, concentration=0.05%	55
Figure 24:	Graph showing shear-thickening behavior of PVF ₂ for T=104°C, concentration=0.3%	56

ACKNOWLEDGEMENTS

I would like to thank all the people that made this thesis possible. I thank Dr. A.J. McHugh for giving me the opportunity to research and for his advice. I thank everyone in Dr. McHugh's group for their constant support and assistance. I would especially like to mention Stanley Tam and wish him good luck with this project. Finally I want to thank the glass and machine shops for their help in building much of the apparatus.

This research was financially supported by a grant from the National Science Foundation. (DMR 84-04968)

Flow-Induced Crystallization of PVF₂

I INTRODUCTION

Flow-induced crystallization is a phenomenon which occurs only in polymers. Under quiescent conditions, a polymer crystallizes from dilute solution in the form of lamellar shaped crystals. This process has been well documented and is well understood.(1) By imposing a hydrodynamic field, a polymer can be crystallized in the form of long, thin fibers. This behavior can occur at temperatures well above the lamellar crystallization temperature.(2)

Pennings et.al.(2,3) first noticed this behavior in the early 1960's with linear high molecular weight polyethylene; since then a number of other polymers have been crystallized by this method, including isotactic polypropylene(4), polyethylene oxide(5), isotactic polystyrene(6) and polyoxymethylene(7). All of these fibers have the same "shish-kebab" morphology, a central filament consisting of more or less extended chains and lamellar overgrowths with folded chains.(3,8)

Polyvinylidene fluoride (PVF_2) has been studied extensively in the last 10-15 years, with most studies having been concerned with the conformational crystal structure of the PVF_2 molecule, which has been the source

of sharp debate. A total of 4 different crystalline polymorphs are known(9), the alpha, beta, gamma and delta phases. PVF₂ also has a number of interesting electrical properties (piezo and pyroelectricity) which has already led to a number of very useful technological applications in the electronics industry. However, to date, there have been no reported studies on the flow-induced crystallization behavior of this material.

This thesis details a study on flow-induced crystallization of PVF₂. Only one set of experimental conditions were found that produced fibers consistently. The fibers produced were characterized using Differential Scanning Calorimetry and optical microscopy. Shear thickening experiments were performed on the PVF₂ solutions to determine if the necessary conditions were present for fiber formation. It is hoped that the results of this study will be useful in further work to produce PVF₂ fibers.

II BACKGROUND

A) Flow-Induced Crystallization

1) Formation

Flow-induced crystallization was discovered over 20 years ago for the system polyethylene in xylene. Pennings et.al.(2) observed that for solutions stirred in a Couette geometry at temperatures slightly above the normal quiescent crystallization temperature and at rates greater than approximately 300 r.p.m., long continuous fibers formed. Since then, this phenomenon has been studied extensively in a number of different geometries.

Fibrous crystallization was noticed in conjunction with the formation of halos, which were described as concentric rotating rings which rotate in a plane perpendicular to the stirrer. The onset of halos has been successfully correlated with the onset of fiber formation, i.e. if no halos are seen, then no fibers will form.(10) The onset of halos also corresponds to the onset of a secondary flow pattern, so called Taylor vortices.

Taylor vortices occur at higher rotor speeds as a result of the centrifugal forces due to large circular fluid motions.(11) The simple shear flow present at lower stirrer speeds will now contain small circular eddies where

elongational flow will exist as seen in Figure 1. This type of flow was characterized by G.I Taylor(12) in the early 1920's. The condition for formation of the eddies is seen in a critical Reynolds number R_C . R_C is given by the relationship(11)

$$R_C = 41.3 * \frac{R_1}{R_2 - R_1} \quad (1)$$

$$R_C = \frac{2 R_1 (R_2 - R_1) n_{crit}}{v} \quad (2)$$

in which

R_1 = Radius of the inner cylinder

R_2 = Radius of the outer cylinder

v = Kinematic viscosity of the fluid

n_{crit} = Critical rotor speed

Pennings (3) also discovered that high shear rates in simple laminar flow without the formation of Taylor vortices were not sufficient to produce fibrous crystallization. Giesekus(13) noticed that vortices can occur at rotation rates as much as 600 times smaller in normal stress fluids than that predicted by the Taylor criterion. Pennings(3) found that high molecular weight polyethylene solutions produced crystals at rotation rates of 380 r.p.m. where the Taylor criterion predicted the

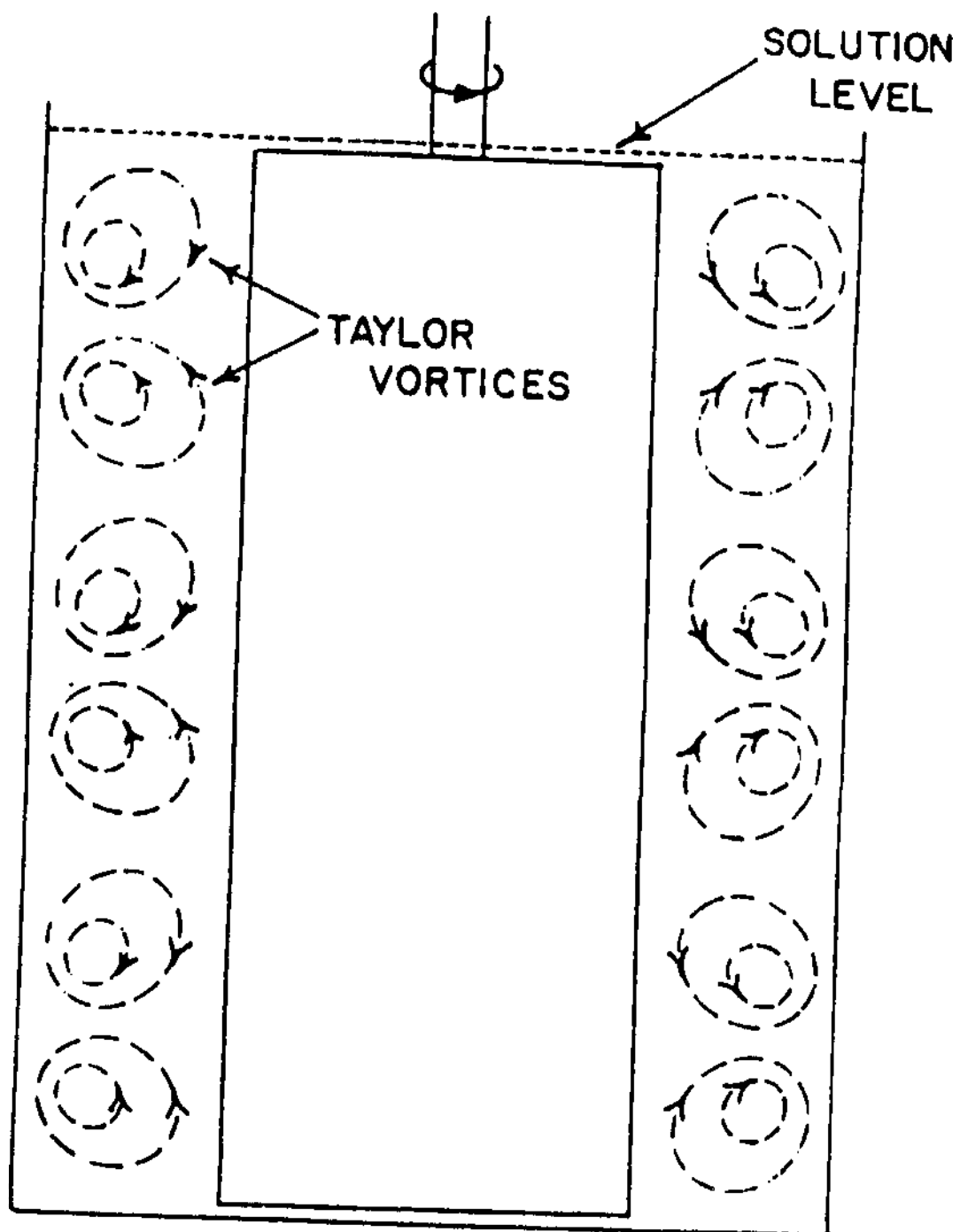


Figure 1. Secondary Flow Pattern in a Couette Annulus

the secondary flow pattern occurring at 1700 r.p.m.. He also found that the solution of high molecular weight polyethylene showed a pronounced Weissenberg effect prior to the first formation of fibers.(14)

Between the Taylor vortices where the stream lines converge, elongational flow components exist. The polymer coils are prevented from rotating which means that they can be continuously extended by the flow.(1) Essentially Pennings concluded that nucleation must occur where the deformation rate tensor has components parallel to the streamlines. Pennings also expected that the Taylor vortices give rise to extensive polymer coil deformations, which would favor nucleation.

The elongational flow is the essential condition for fiber formation. In the following, 3 different methods used to crystallize fibers will be briefly mentioned to point out the elongational flow elements.

The first geometry is that of impinging jets studied by Frank, Keller and Mackley.(15) The experimental geometry is shown in figure 2. These authors analyzed the flow system and found a region in the plane of symmetry at the center of symmetry where extensional flow occurs without rotation. They observed that fibers crystallized where longitudinal elongation occurred without rotation. They also observed birefringence at solution concentrations

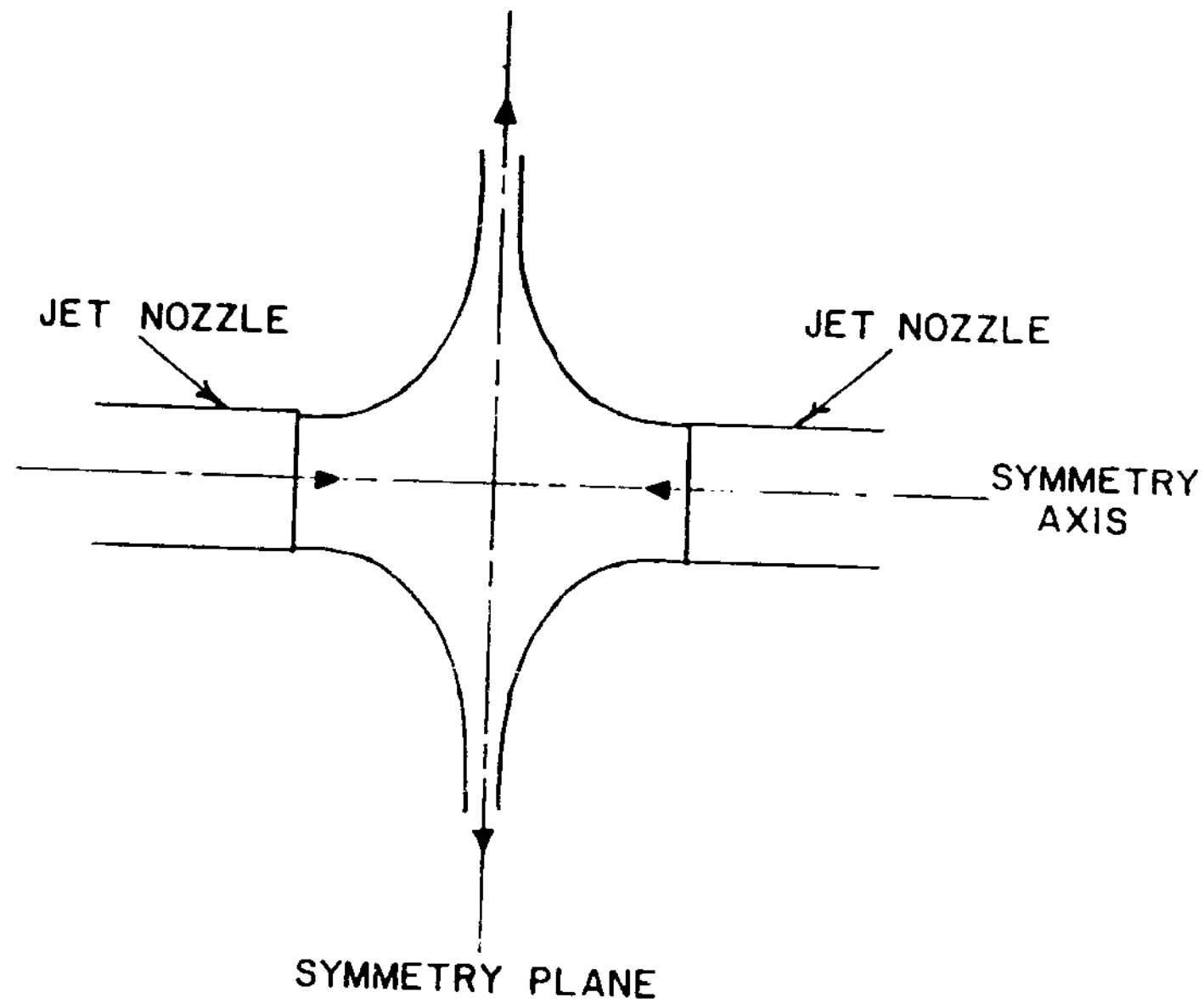


FIGURE 2. LINE DRAWING OF FLOW PRODUCED BY IMPINGING JETS

greater than 2 percent though no birefringence was seen at concentrations of 1 percent. The maximum limiting temperature was 112°C.

The next two methods use seed crystals in order to produce the elongational flow. The seed crystal is usually a thin polyethylene fiber having a cross-sectional area on the order of .01mm² and is usually mounted in a hypodermic needle or a thin filament which allows for control of the seed location. The two techniques are the surface growth technique and the tubular flow technique.

The surface growth technique utilizes a Couette geometry with a side arm attached and can be carried out either continuously or statically. In the continuous mode the seed crystal, which is attached to a take-up roll by a thin filament, is pushed through the side arm after the inner cylinder is rotating. The seed crystal is then aligned by the flowing solution and pushed towards the rotor surface. After contact with the surface, the seed crystal begins to grow and the take-up roll is started. Growth can be maintained for periods of time up to days provided the take-up rate is maintained equal to the steady state growth rate of the crystal. Figure 3 illustrates the continuous mode. The static growth method uses the same seed crystal and side arm arrangement, but the rotor is

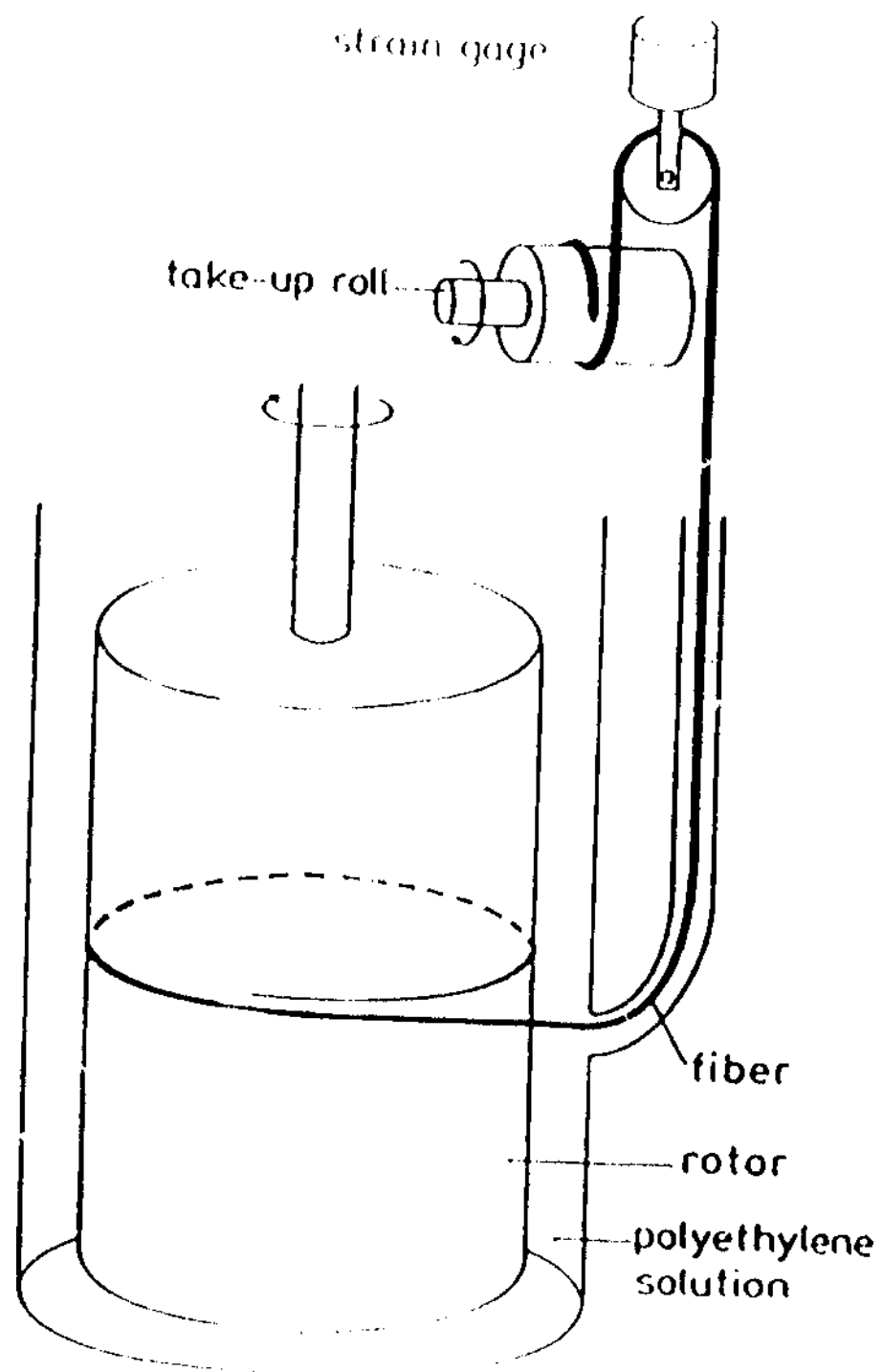


Figure 3. Surface-growth apparatus

rotated for a set time, then turned off and the fiber removed. (17)

A number of studies using this method have been made. (17,18,19,20,21) Most studies are concerned with the rate of fiber growth. For example, Rietveld and McHugh(17) found a maximum growth rate of 300 cm/min for a rotor speed equal to 1300 r.p.m.. They also found a marked dependence of the fiber growth rate on the rotor surface, the significance of which will be discussed later.

Pennings et.al.(22) found that simple shear flow was sufficient to induce crystallization in the surface-growth technique. Mackley(23) carried out a theoretical analysis of the flow-field of a fibrous crystal held stationary in a flowing polymer solution. He assumed that the growing fiber tip may be approximated by a rigid ellipsoid with the major axis oriented parallel to the flow and held stationary (see Figure 4). He also assumed that the ratio of the major to minor axis would be large and calculated from a Stokes flow solution that at a freestream velocity of 10 cm/sec, an extensional flow gradient of $10^5-10^7 \text{ sec}^{-1}$ can exist near the seed downstream surface. This suggests that the extensional flow necessary for fiber formation occurs at the fiber tip, and is not caused by the bulk solution. (17)

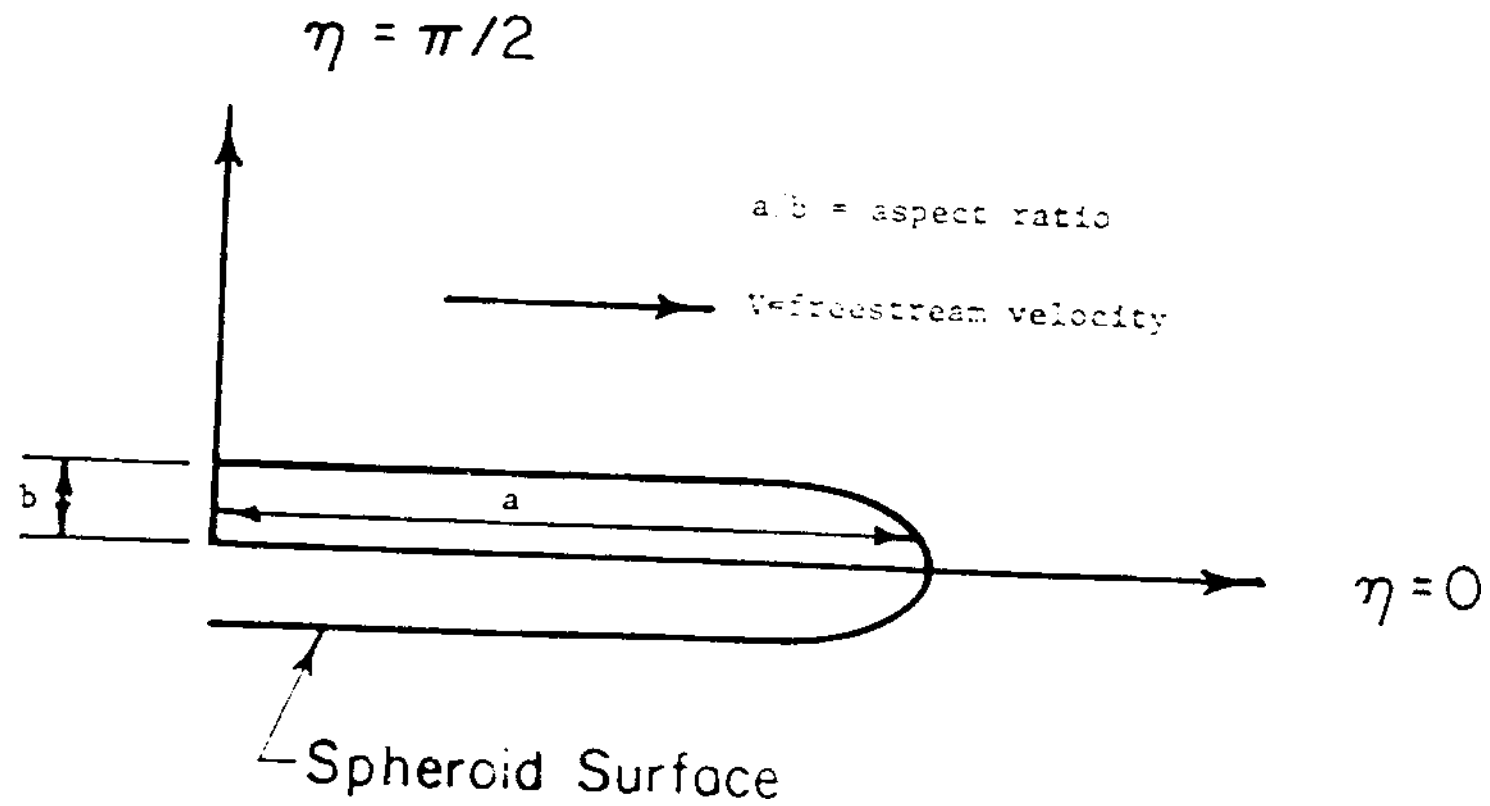


Figure 4. Illustration of model used by Mackley

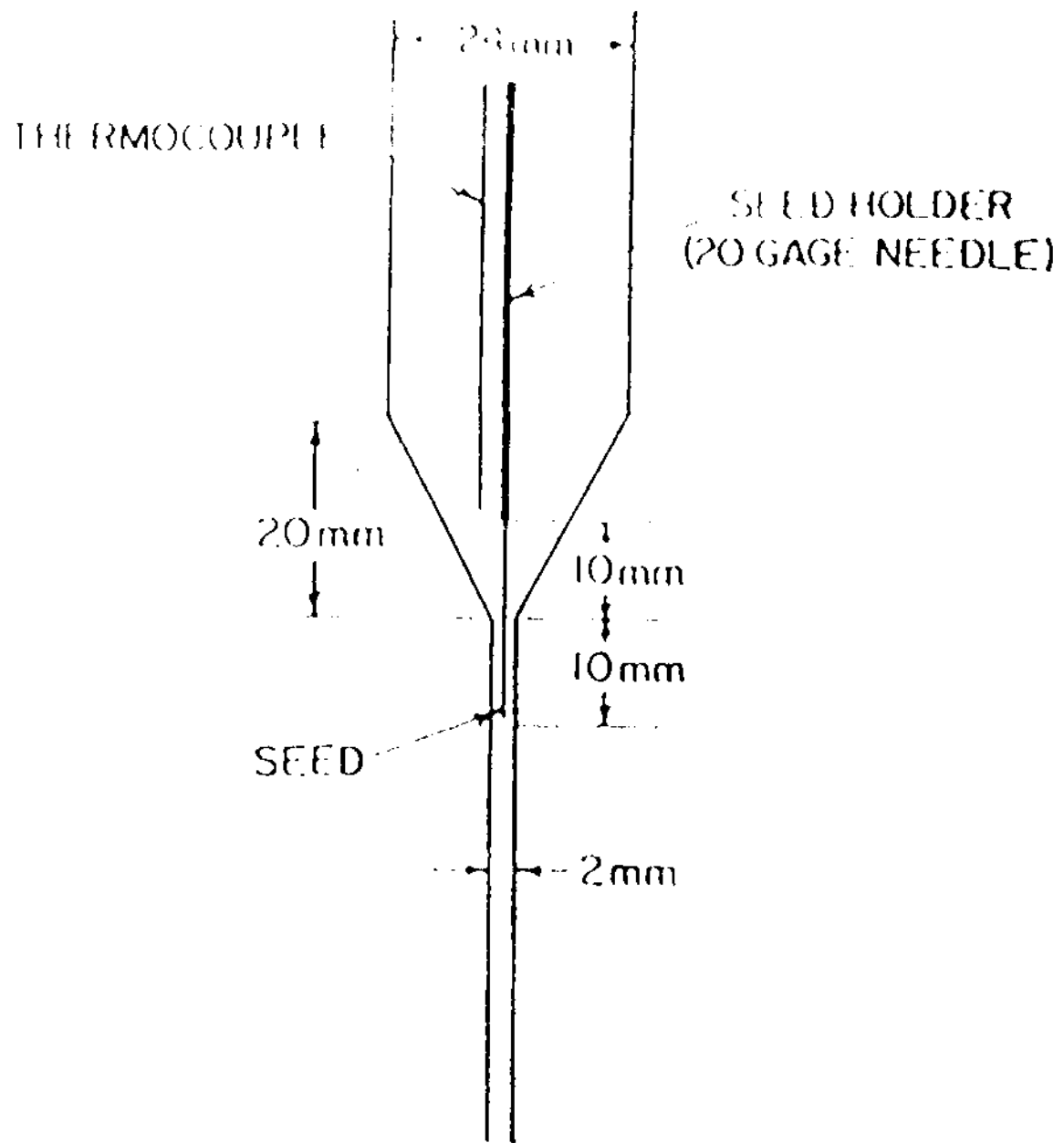


Figure 5. Tubular-growth apparatus

The tubular flow technique uses the apparatus as shown in Figure 9. The heated polymer solution is allowed to flow past the fiber seed crystal and the growing fiber is observed. Recent improvements in procedure, i.e. video cameras and optical birefringence, have allowed Rietveld and McHugh(16,24) to observe the fiber transformation sequence. They found that initially pure polymer forms an unoriented precursor which is anchored to the seed and this precursor transforms itself into the crystalline state through the growth of oriented crystals induced by stress transmitted from the flowing solution. It was concluded that physical entanglements in the precursor acted as crosslinks. The elongational flow here can occur in two regions. The fiber tip causes elongational flow, Mackley's analysis(23) does not depend on the geometry of the flow. The tapered entrance region also provides a region of elongational flow. On the other hand, once the anchored precursor develops, the elongational force necessary for crystallization is transmitted to it by the shearing drag of the surrounding flowing solution.

A number of investigations have been carried out on the nature of the rotor surface and the effect it has on the nucleation of fibers.(17,21,25) All of these studies have employed the surface growth method. Teflon and other highly adsorbent surfaces have been found to promote fiber

highly adsorbent surfaces have been found to promote fiber formation much more than glass. Pennings and Torfs(21) found that adsorption of very high molecular weight polyethylene on the rotor surface plays an essential role in nucleation. They concluded that the crystal grows in a gel layer which adheres to the rotor surface. Of course, polyethylene adsorbs on teflon more readily than on glass, hence fiber formation is promoted.

They also discovered that polyethylene solutions gel when cooled, if they are stirred at elevated temperatures, while an unstirred control polyethylene solution will not gel. A time factor is associated with gelation. They discovered that gel would not form upon cooling if the solution was stored at 134°C for at least 4 hours after stirring had been halted. They also found that longer times were necessary at lower temperatures. The time scale was rather long, certainly greater than that associated with molecular relaxation or diffusion. The highest temperatures at which gels would form was found to increase with increasing stirrer speed. Thus, gel formation correlates with fiber formation, since only solutions capable of gelation can form fibers.

Torfs and Pennings(21) proposed a tail-train loop model to explain the adsorbed behavior (see Figure 6). Essentially large polymer molecules are adsorbed on the

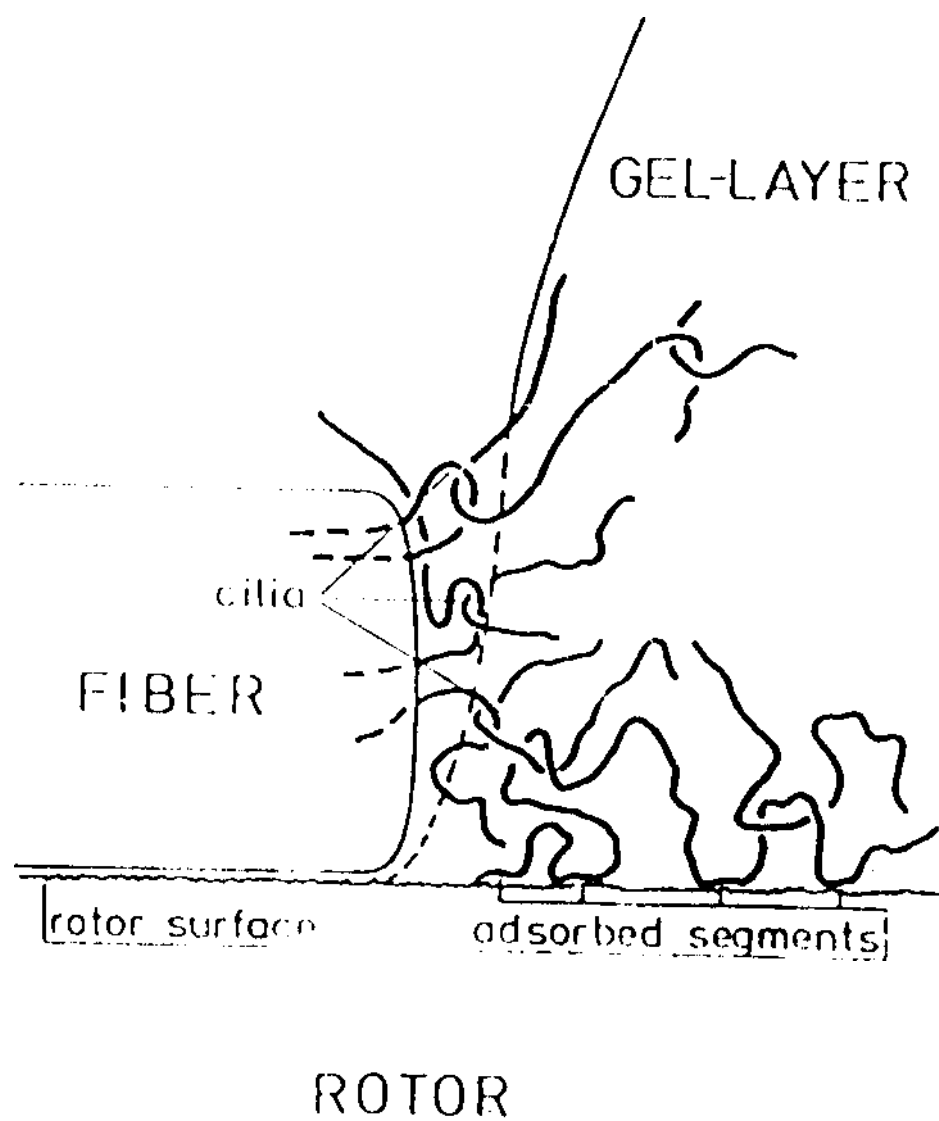


Figure 6. Trail-train loop model
The adsorbed segments form entanglements
which provide the nucleation for fiber growth.

rotor surface at multiple points. This leads to entanglements between the adsorbed polymer layer and other polymer molecules, causing the formation of a gel-layer. This leads to nucleation, which in turn leads to fiber formation. In support of this theory is the molecular weight fractionation that takes place in any fiber formation. Of course, large molecules would be more likely to become entangled in the gel-layer, hence they would be found preferentially in the fiber.(18) This molecular weight fractionation will be further discussed later in this thesis.

Pennings and Torfs(21) concluded that the fibers that form are caused by the stretching of the network structure (gel-layer). This process is shown in Figure 7. The elongational flow field is of course the cause of the stretching necessary for the fiber formation. It is this network structure which causes the build-up in shear stress which is the subject of a recent PhD thesis by Vrahopoulau.(26)

In this case it was found that polymer solutions exhibited shear thickening behavior under certain flow conditions, i.e. the reduced viscosity increased and showed a maximum when plotted against the shear rate. Figure 8 shows a representative graph of data taken using a standard capillary flow device. The shear thickening behavior they

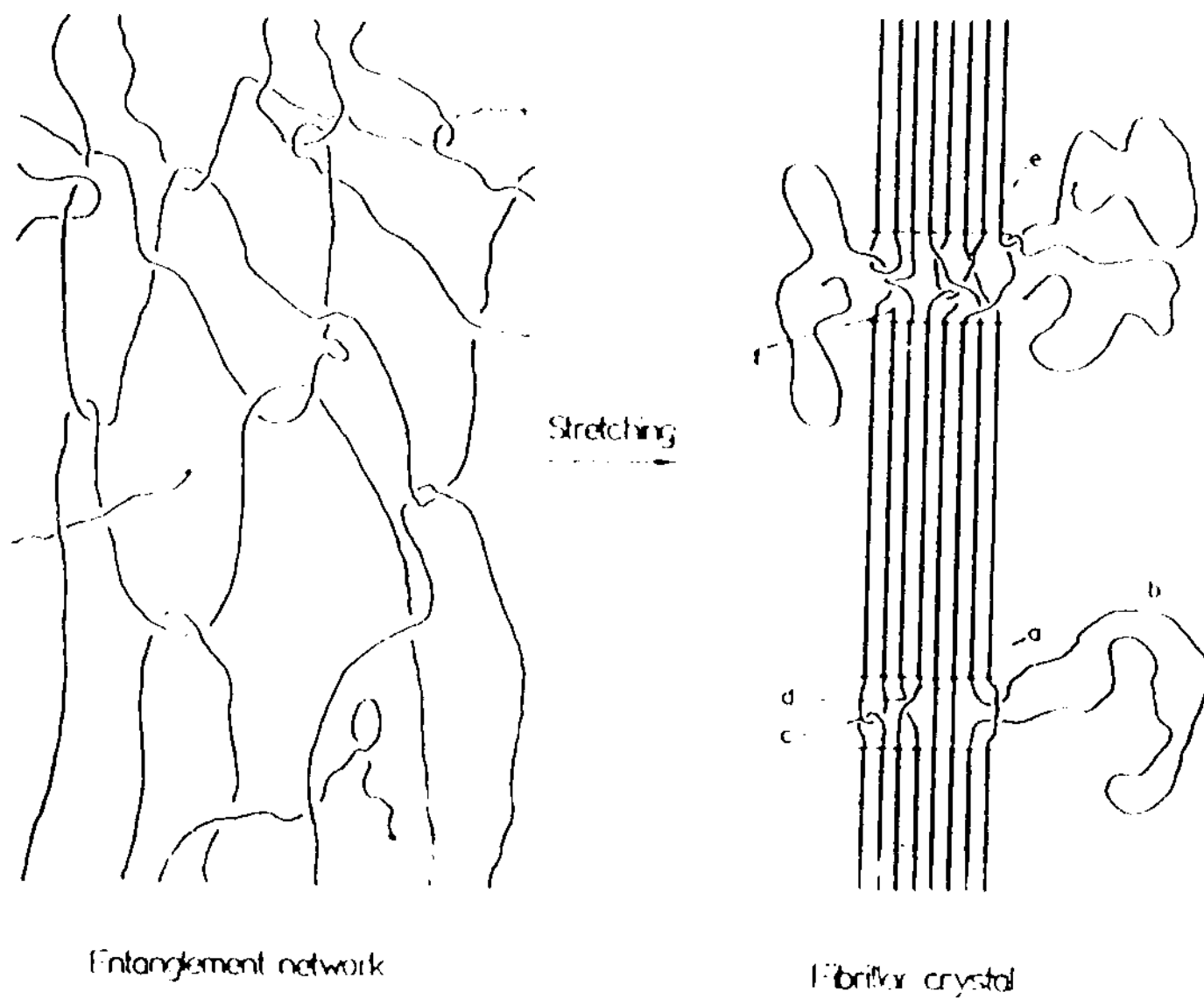


Figure 7. Transformation from network to fiber

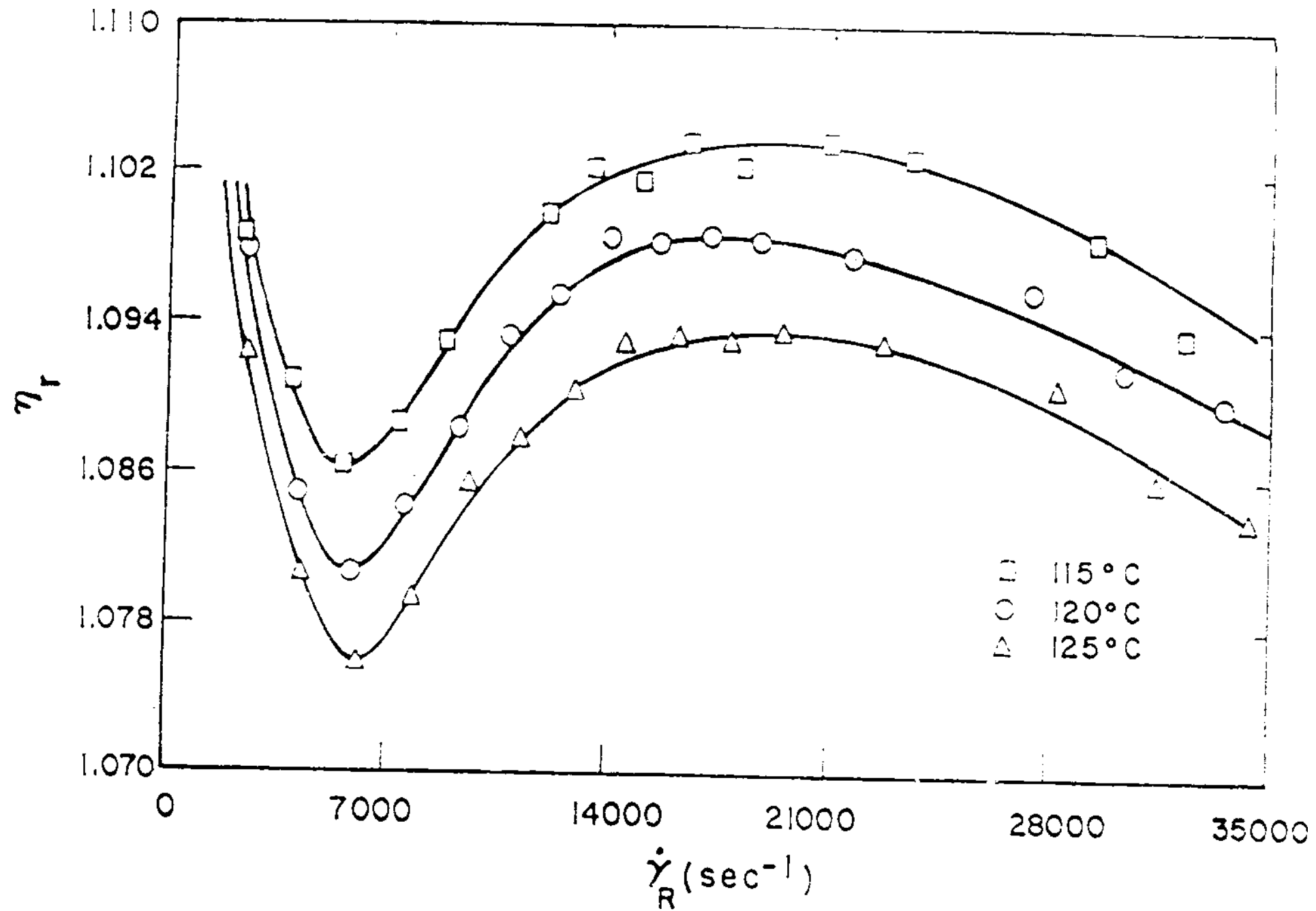


Figure 8. Shear thickening behavior
(UHMWPE in xylene, concentration=0.005%)

believed was an indication of network formation; the same network formation is indicative of the entanglements necessary for fiber formation. It was concluded only those polymers that exhibited this shear thickening behavior were able to form precursors and thus crystallize as fibers.

2) Morphology and Molecular Weight Fractionation

The fibers produced all exhibit the basic shish-kebab morphology, independent of the external flow-field. A shish-kebab consists of a long chain (shish) with lamellar overgrowths (kebabs). Figure 9 is an illustration of a shish-kebab while Figure 10 shows a typical electron micrograph (taken from Pennings, Mark and Kiel(3)). The shish can be thought of as extended (or nearly extended) polymer while the kebab is seen as lamellar overgrowths. Studies of the morphology indicate that the lamellar overgrowths are not simply deposited on the extended polymer, rather they are incorporated into the backbone structure.(27)

The dimensions of the shish-kebab vary with macroscopic flow conditions as well as post crystallization thermal history. The kebabs are on the order of 10 microns wide and the central shish is on the order of 0.5 microns or less.(8) The distance between the kebabs after washing is generally on the order of 15 microns.

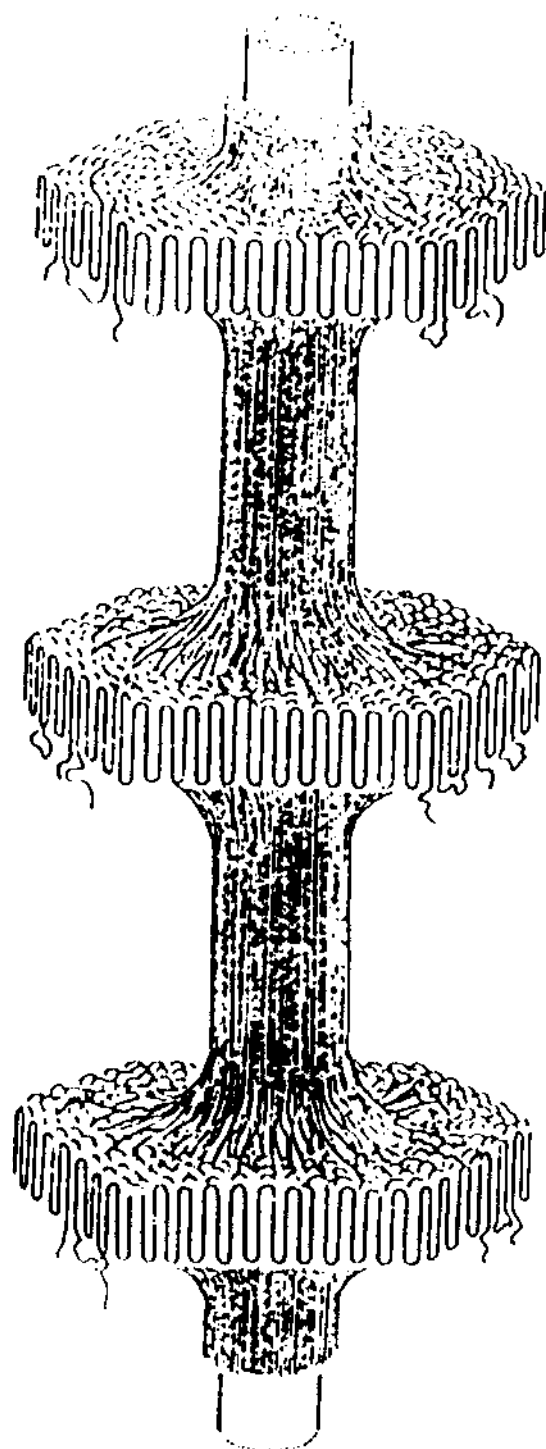


Figure 9. Shish-kebab morphology



Figure 10. Electron micrograph of polyethylene shish kebabs grown from a 5% solution in xylene at 104.8°C.

Washing with acetone removes a large amount of the lamellar overgrowth, but there is always some overgrowth left, which indicates an incorporated phase.

Crystallization temperature affects the kebab size and spacing. The spacing between the kebabs increases while their size decreases as temperature is increased. At very high crystallization temperatures (112°C) for polyethylene in xylene, nearly 20°C over the quiescent crystallization temperature, the fibers appear to be smooth with no lamellar overgrowth.(19) The melting peak behavior of shish-kebab fibers shows a broadening over the usual bulk crystallized sample in a DSC trace. The sample can exist in a superheated state i.e. melting will occur at temperatures greater than the highest seen in a bulk crystallized sample. Melting has been found for polyethylene at temperatures equal to the theoretical melting temperature of infinitely extended crystals. The DSC also indicates that the material with the high thermal stability somehow transforms much of the sample into a superheatable form.(8)

Molecular weight fractionation is also seen in the fibers. In general, flow-induced crystallization is not a very good method of fractionation, large amounts of low molecular weight material are contained in the fiber. For example, Pennings(28) crystallized polyethylene from a

solution with $M_w/M_n=29$, while the original sample had $M_w/M_n=13$. The M_w value increased by a factor of 2.5. He also found that the fractionation has a binodal distribution, one part due to the high molecular weight material and one part due to the low molecular weight material. Washing the fibers caused much of the low molecular weight material to disappear, apparently the low molecular weight polymer was not actually part of the fiber. At higher crystallization temperatures; however he found that only the high molecular weight fraction will crystallize.

The mechanical properties of the fibers are significantly different than the bulk crystallized material. Both the Young's modulus and the ultimate tensile strength were greatly increased over polyethylene structures crystallized from the melt or from solution. As the crystallization temperature for the fibers increased the modulus and the tensile strength at break also increased. The highest temperature crystallized fibers (119°C) had a modulus and tensile strength at break very close to that theoretically calculated for an ideal polyethylene crystal oriented parallel to the chain direction. (25)

b) PVF₂

Polyvinylidene fluoride (PVF₂) has been one of the most widely studied polymers in the last 10-15 years, over 1000 papers have been published in the last 15 years.(9) Many of the papers concern the complicated polymorphism; and a good deal of debate has taken place in the literature about the subject. The main reason for all of this study is the potential use for PVF₂, its unusual electrical properties in certain crystal forms would make the polymer ideal for transducers and hydrophonic devices over wide frequency ranges.

The interesting electrical properties in PVF₂ arise from its pyro(29) and piezoelectricity.(30) Pyroelectricity occurs if a material show a change in polarization with a change in temperature, piezoelectricity occurs if a mechanical stress produces a change in electrical polarization (or vice-versa). Both effects are a result of macroscopic polarization applied to the polymer, transforming the material into an electret. An electret is a term used to describe the electrical analogue of a magnet i.e. a permanent polarization exists in the material. Polyvinylidene fluoride is the first material to be developed that has the mechanical properties necessary for commercial applications as an electret.

PVF₂ consists of the repeat unit [CH₂-CF₂]. Two arrangements are possible, a head to tail [CH₂-CF₂-CH₂-CF₂] or a head to head [CH₂-CF₂-CF₂-CH₂]. The head to tail form is preferred and also has more useful molecular properties. Four different confirmed crystalline phases have been found for PVF₂, with 2 or 3 more recently reported in the literature.(31) The four different polymorphs are designated alpha, beta, gamma, delta or II, I, III, IV_p.

The alpha phase is most common, this phase is available commercially. Formation of the alpha phase occurs at moderate to high undercoolings from the melt, i.e. at temperatures less than 150°C.(32-34) The alpha phase also forms during single crystal precipitation from certain solutions, such as dimethylformamide, monochlorobenzene, a xylene-acetone mixture, and cyclohexanone.(31) The backbone is a slightly distorted tg⁺tg⁻ structure (a 2₁ helix). The t angle is 179° while the g angle is 45°. A schematic of the backbone structure is shown in Figure 11

The unit cell of the alpha form is shown in Figure 11 also. The cell is orthorhombic with a=4.96Å, b=9.64Å and c=4.62Å.(35) The PVF₂ molecules are polar; however the alpha unit cell has the dipole moments arranged anti-parallel, hence the alpha form is not pyro or piezoelectric. The alpha form is also the most energetically favored of all the forms in a nonelectrical

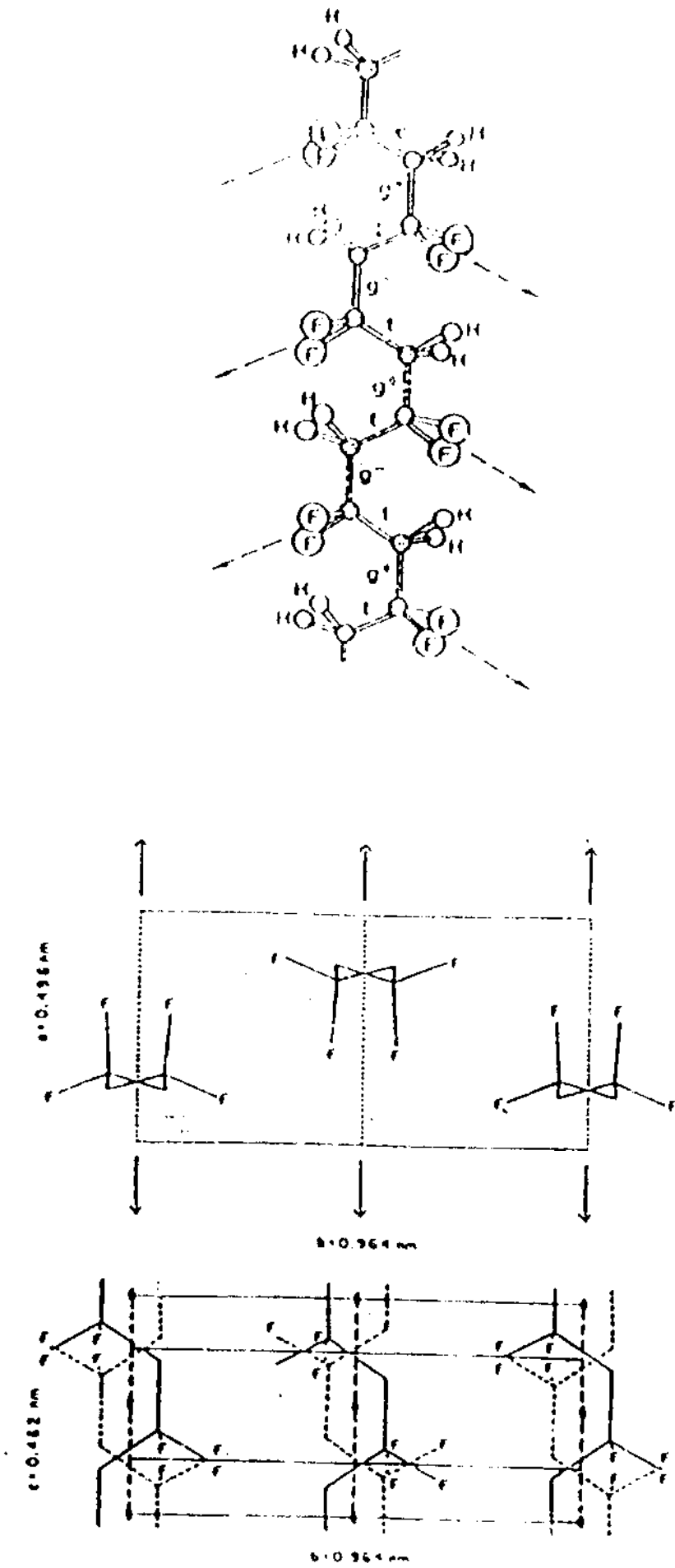


Figure 11. Molecular backbone and unit cell for the alpha phase

environment, because no steric strains exist between the fluorines and the stress between the hydrogen and the fluorine is minimal.(36)

The beta phase has the most potential commercial applications because the unit cell for this phase is polar. The most common method of crystallization is mechanical deformation of films at temperatures less than 80°C. The backbone structure is an all trans arrangement as shown in Figure 12. The unit cell (also shown in Figure 12) of PVF₂ is orthorhombic with constants $a = 8.58 \text{ \AA}$, $b = 4.91 \text{ \AA}$ and $c = 2.56 \text{ \AA}$.(37) The all trans arrangement causes the fluorine atoms to come closer together than the van-der Waals radius allows. Galperin(38) et.al. theorized that the CF₂ groups were deflected to the right and left of the zig-zag, as the dotted lines in the unit cell of Figure 12 suggest. The angle of deflection was calculated to be 7°. This hypothesis was later confirmed through x-ray diffraction and potential energy calculations. The dipoles are parallel in the beta phase, hence the unit cell is polar.

The gamma phase can be thought of as a mix of the alpha and beta phases. The phase is produced by high temperature annealing of alpha PVF₂(34), high temperature crystallization from the melt or high pressure crystallization from the melt.(40,41) The gamma phase will

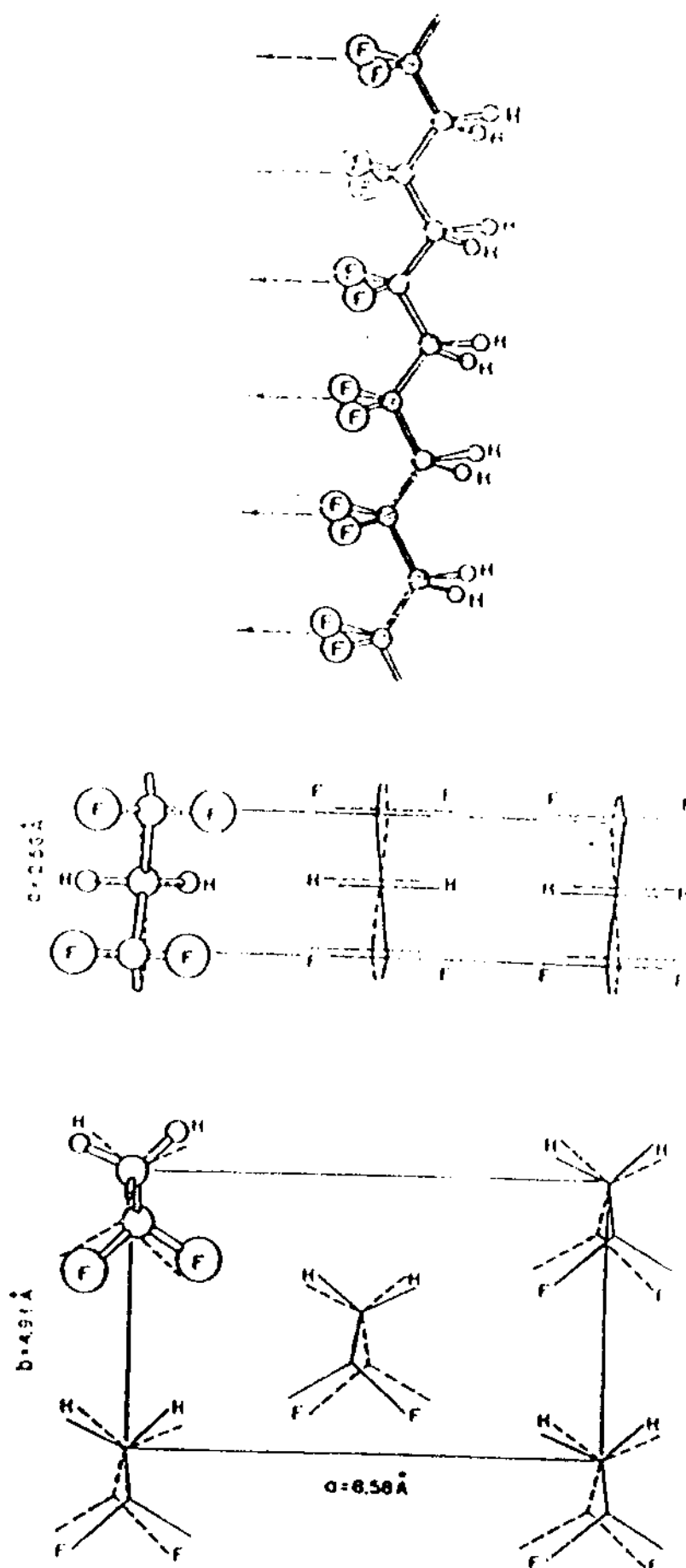


Figure 12. Molecular backbone and unit cell for the beta phase

crystallize from solution using the solvents dimethylacetamide(41) or dimethyl sulfoxide.(42) The backbone of the gamma phase is t_3gt_3g .

The gamma phase can be thought of as a kinked beta phase, with the kinks occurring at every fourth bond along the chain. The unit cell of the gamma form is a source of sharp debate, Lovinger(43) proposed a monoclinic structure with $a=4.96^{\circ}\text{A}$, $b=9.00^{\circ}\text{A}$, $c=9.20^{\circ}\text{A}$ and $\beta=93^{\circ}$. Weinhold, Litt and Lando(44) proposed an orthorhombic structure with $a=4.96^{\circ}\text{A}$, $b=9.66^{\circ}\text{A}$ and $c=9.18^{\circ}\text{A}$. Weinhold et.al. claimed later that both unit cells may exist in the gamma phase. The delta phase was recently discovered. By poling the alpha phase under a high electric field, an inversion of dipole moments occurs resulting in a polar alpha phase. The unit cell was found to be orthorhombic with $a=4.96^{\circ}\text{A}$, $b=9.64^{\circ}\text{A}$ and $c=4.62^{\circ}\text{A}$. This unit cell is the same as the alpha phase, the difference lies only in the chain packing. The backbone structure is also the same.(46)

Polymorphic transitions also occur in PVF_2 , as in many other polymers. There are three types of transformations: electrically induced, thermally induced or mechanically induced. Figure 13 details the polymorphic transitions of PVF_2 .

The melting behavior of PVF_2 is very complicated, for a variety of reasons. As documented earlier, a large number

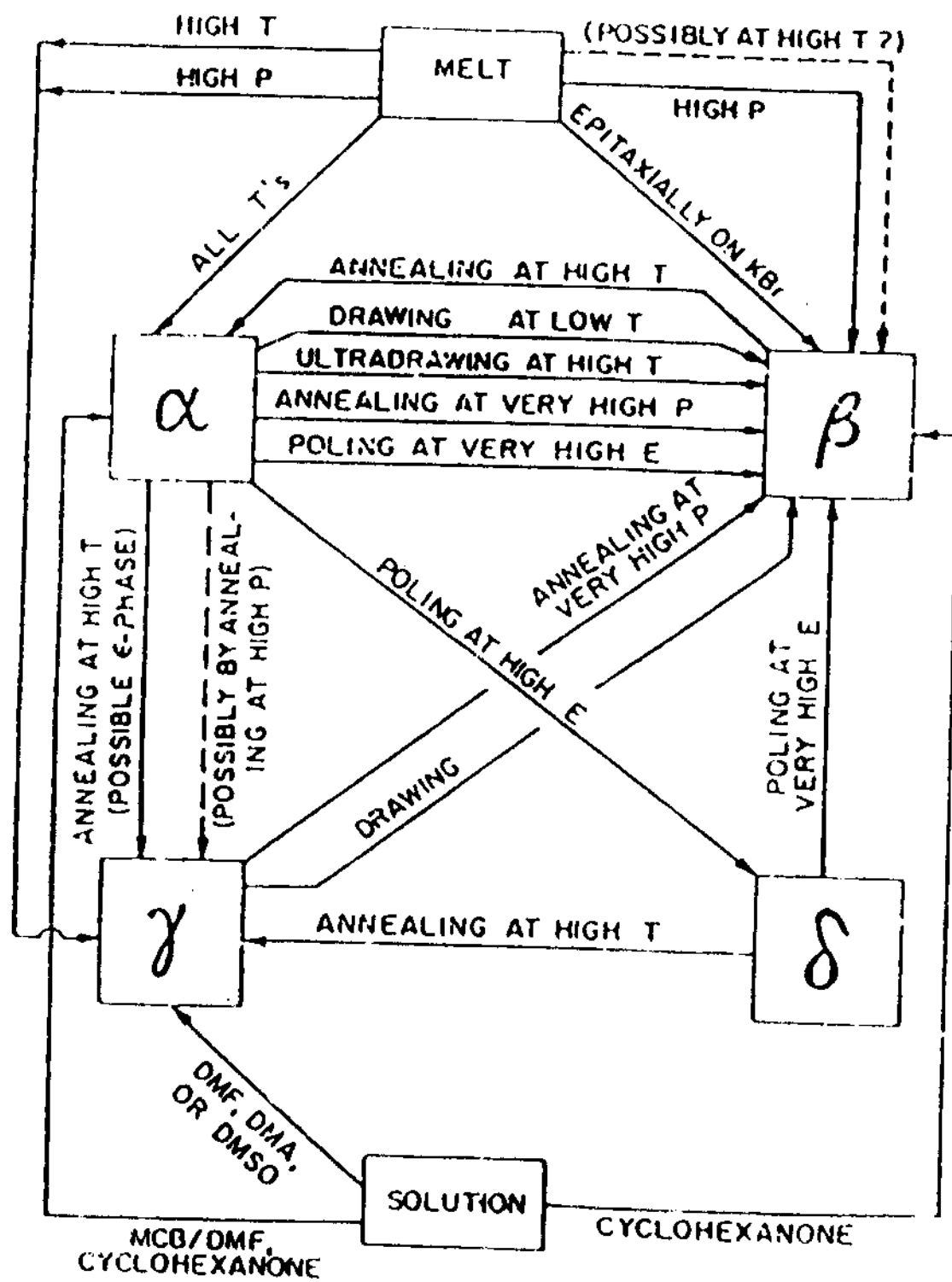


Figure 13. Polymorphic transitions of PVF₂

of polymorphs and interconversions between them complicate melting behavior. Head to head and tail to tail defects also complicate the melting behavior. No true melting point for PVF₂ exists, 160°C-200°C is the usual range. The exact value depends on the history of the material. The thermodynamic melting point of the alpha phase (the most stable form) was theoretically calculated to be 200.9°C.(9)

PVF₂ will degrade at temperatures over 150°C in the solid state. The degradation involves primarily a dehydrofluorination. The polar forms were found to degrade much easier than the non-polar forms. The degraded material is much darker than the normally clear PVF₂.

III Experimental

A) Materials

The PVF₂ used was Kynar 461 obtained from the Pennwalt Corporation with Mw=534,000 and Mn=11,000. In both the shear thickening and the fiber growth experiments, .25wt% of Santonex, an antioxidant, was also dissolved in the solution. The solvent used in all solution experiments was dimethyl phtalate obtained from the Aldrich Chemical Company.

B) Fiber Growth Experiments

A Couette apparatus was used, Figure 14 shows a cross-sectional view of the apparatus. The inner cylinder was constructed of teflon or glass, with diameter 5.5 cm. The inner cylinder was connected to a motor which allowed for control of the stirrer speed. The outer cylinder was made of glass with diameter 7.0 cm. A special 60/50 glass joint was used in order to minimize dead air space. The teflon bearing and the teflon rotor were used to stabilize the apparatus. The entire device was submerged in a silicone oil bath, so that the temperature of the solution could be controlled to $\pm 0.1^{\circ}\text{C}$ by a Precision Temperature Regulator manufactured by the Bayley Instrument Company.

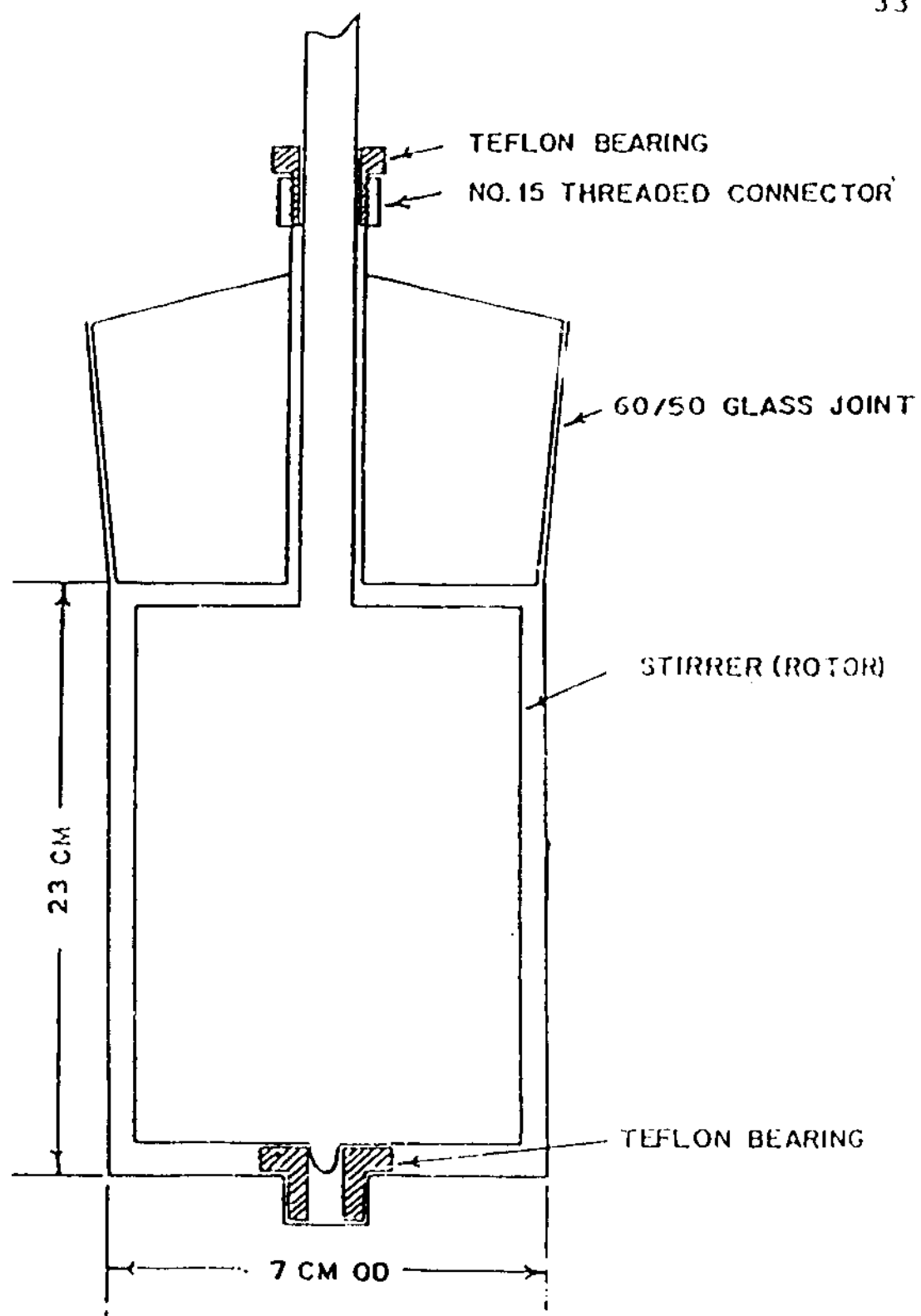
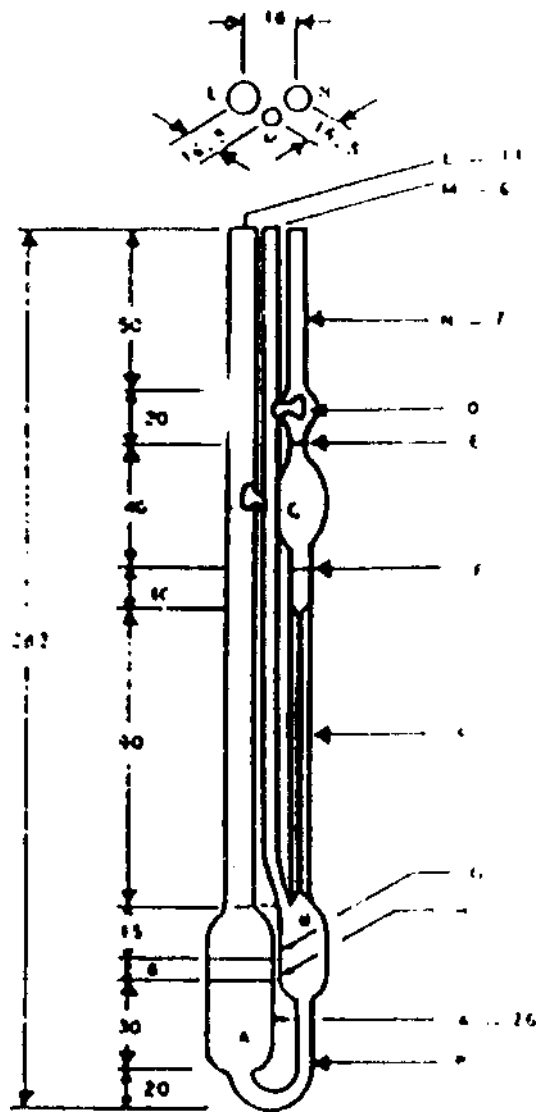


Figure 14. Couette apparatus

The PVF₂ was dissolved, along with the Santonex, at a temperature between 180-185°C. Concentrations of PVF₂ ranged from 0.1 to 0.4. The solution was cooled to the desired temperature. The inner cylinder was then inserted, and the motor started. Shaking, rubbing and vibrating were minimized by different positioning of the apparatus. After the desired time period, the inner cylinder was removed and both cylinders plus the solution were examined for any evidence of fiber growth.

C) Shear Thickening Experiments

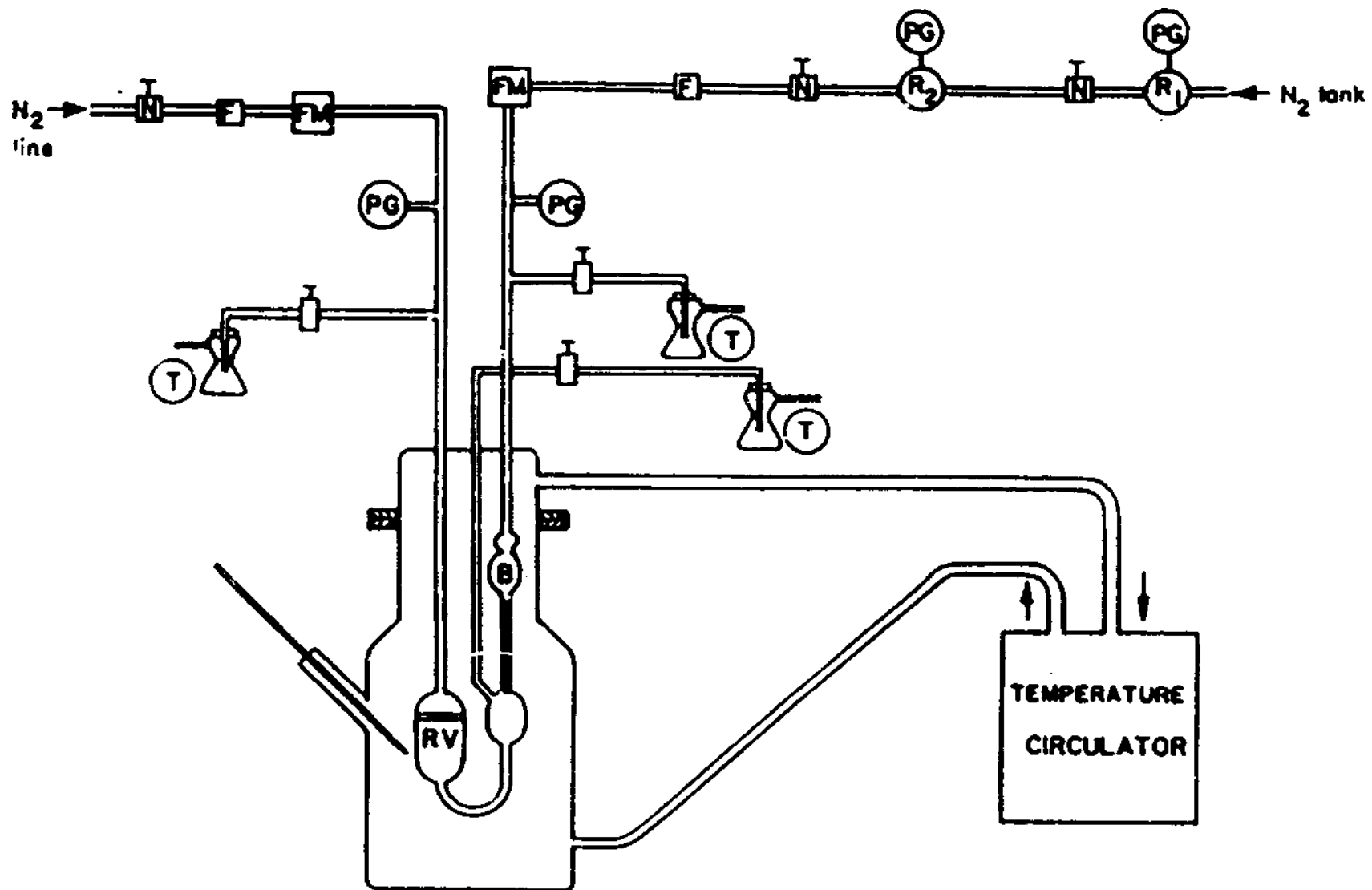
Shear thickening experiments were conducted using an Ubbelohde viscometer (No. 0217) obtained from the Cannon Instrument Company. The capillary diameter was 0.24 mm and the capillary length was 90 mm. (Figure 15) This same apparatus was used in reference 26. The volume of the timing bulb was 1.06 ± 0.01 ml. (26) The whole apparatus was submerged in a constant temperature reservoir of circulating oil. The oil was circulated from top to bottom by a temperature controlled circulator purchased from the Polyscience Corporation. (Figure 16) A thermometer was inserted with its bulb near the lower reservoir of the viscometer to measure the temperature of the apparatus to $\pm 0.5^\circ\text{C}$. The PVF₂ solution was introduced into the lower reservoir through the use of a syringe. Care was taken to



- A lower reservoir
- B suspended level bulb
- C timing bulb
- D upper reservoir
- E, F timing marks
- G, H filling marks
- L mounting tube
- M lower vent tube
- N upper vent tube
- P connecting tube
- R working capillary

(All dimensions are in millimeters.)

Figure 15. Ubbelohde viscometer



F : Filter	N : Needle valve
FM : Flowmeter	T : Trap
PG : Pressure gauge	B : Viscometer bulb
R ₁ , R ₂ : Pressure regulators	RV : Reservoir

Figure 16. Viscometry apparatus

insure all the PVF₂ was dissolved before being transferred into the lower reservoir. The dissolution temperature was the same as the temperature used for the experiment and the solvent was DMP. To transfer the solution from the lower reservoir to the timing bulb, nitrogen gas from a house line was used. Nitrogen gas from a cylinder was used to provide a pressure drop across the capillary. The magnitude of the pressure drop was varied to provide different shear rates.

Elution time was measured as a function of applied nitrogen temperature. The two timing marks were used to calculate the elution time. The pressure was varied between 0-50 torr, with 5 torr intervals and between 60-160 torr, with 10 torr intervals. Using this range shear rates up to 35,000 s⁻¹ could be obtained. The apparatus was calibrated with pure solvent at the temperature of interest.

Reproducibility of the data was checked 2 ways, Spot checks of pressure were made, i.e. a run at 70 torr would be followed by a run a 20 torr. The runs were also made from low to high pressure and high to low pressure.

The data was reduced using a rather lengthy procedure fully described in reference 26. The reduced viscosity and the shear rate were found by the following equations.

$$n_r = \frac{4t_r}{3 + (1/t_r) \frac{dt_{soln}}{dt_{solv}}} \quad (3)$$

$$\dot{\gamma}_r = \frac{4V_{tb}}{\pi R^3 n_r t_{solv}} \quad (4)$$

where

n_r = relative viscosity

t_{soln} = elution time of polymer solution

t_{solv} = elution time of polymer solvent

$t_r = \frac{t_{soln}}{t_{solv}}$

$\dot{\gamma}_r$ = shear rate at wall of capillary

R = capillary radius

V_{tb} = volume of timing bulb

A computer program was written to work up the data, see Appendix 1.

D) DSC and Optical Microscopy

The Differential Scanning Calorimetry experiments were performed with a Dupont 910 Differential Scanning Calorimeter equipped with a Dupont 1010 Thermal Analyzer. Sample size was between 5 and 10 milligrams.

A Nikon 104 polarizing microscope provided magnification to allow observation of the sample.

Photomicrographs were taken with a Nikon 35 mm camera attached to the microscope with an optical extension tube.

IV RESULTS AND DISCUSSION

A) Fiber Growth

The experimental conditions under which fibers could be produced were found to be very limited. Very long stirring times within an extremely narrow temperature range produced fibers, and at one stirring rate. The long shearing times caused a number of experimental problems with the teflon rotor. Rubbing would occur and foreign matter would discolor the solution, causing the solution to eventually become an opaque black. This rubbing would primarily occur between the metal rotor arm (connected to the inner rotating cylinder) and the teflon bearing that screwed into the number 15 threaded connector. Removing this teflon bearing caused the rotor to shake too much and as a result a stable flow field could not form. The glass rotor did not need the teflon bearing since it was so light compared to the teflon.

The Taylor vortices appeared as 5 or 6 concentric rings when the inner cylinder was spinning. The location of these rings corresponded to areas where fibrous material accumulated on the rotor whenever this formation occurred. Fibers formed only when vortices were seen; however the

converse was not true, i.e. the presence of rotating rings did not necessarily mean that fibers had formed.

Fibers always accumulated on the inner cylinder and appeared more like a thin layer of gel, rather than as filaments. The extracted mats also took an extremely long time to dry, on the order of a couple of weeks and were not very strong. On removing the rotor, the remaining solution was found to have turned a translucent orange from its original milky white color. Note that foreign matter falling into the solution caused the color to turn an opaque black. In addition, both the glass rotor and the teflon rotor gave this result, thus contamination was not causing this discoloration.

In addition the degree of darkening depended on two factors; the stirring time and the temperature of the crystallization run. Longer stirring times and/or higher crystallization temperatures led to a greater discoloration. On the other hand, unstirred control solutions did not show the discoloration at times as long as 72 hours and at temperatures equal to the fiber crystallization temperatures.

It is believed that the discoloration is due to degradation of the polymer which could severely reduce the molecular weight. As discussed in the background,

degradation of PVF₂ primarily involves a dehydrofluorination. A literature search revealed that little has been published about the degradation of PVF₂ in solution. Bases, such as KOH and dimethyl formamide, are thought to promote degradation(9) leading to solution discoloration very similar to that observed in this study.(47) Further study is clearly needed on this aspect of the experiment to determine what causes the degradation and what effect this has on the molecular weight.

A number of factors, such as temperature, stir time etc., affected the growth of the fibers. The stirring time affected fiber formation in several ways. To begin with a minimum time of 24 hours was necessary to obtain fiber mats. For growth times less than this (i.e. 18 hours) ring shaped deposits formed, however there was never enough material in the deposit to remove as a fiber. With increased stirring time, the amount of the material formed increased; however the thickness of the resulting fiber mats was reduced. Although only qualitatively checked, fibers grown for longer periods also seemed a bit stronger.

The crystallization temperature also had a profound effect on the fiber growth. For example, at 89.4°C, the polymer precipitated as single crystals while at temperatures of 91.6°C, fibers formed. At a temperature of 95.8°C, no fibers formed for stirring times as long as 48

hours. At 93.8°C, ring shaped deposits formed; however not enough material was present to be removed as a fiber. The maximum range for fiber formation was found to be less than 4°C. This is a very narrow range when compared to other olefins such as polyethylene and polypropylene. The range for both polyethylene(3) and polypropylene(48) was over 20°C.

The rate of stirring also had an effect on fiber formation. Surprisingly, only one stir rate (approximately 350 r.p.m.) consistently gave fibers. The weight percent of the solution had little or no effect on the fibers, assuming of course that all of the material could initially dissolve in the solvent at that particular concentration.

The only rotor material that produced fibers was teflon. As indicated in the background, teflon is much more adsorbent than glass and therefore produces fibers much more easily. Given the difficulty already discussed, the fact that glass did not produce fibers was not surprising. Very slight evidence of concentric rings did appear on the glass rotor; however it proved impossible to remove any precipitated material.

Washing with acetone at room temperature had a macroscopic effect on the fibers. Initially the fibers had a manila color which changed to pure white after washing, the same as the color of the original material. A large

amount of the polymer also dissolved in the acetone. Likewise washing tended to loosen the precipitated mat making the fibers more visible i.e. the length to width ratio was greater.

Two things could have caused the manila appearance. Since Santonex, the antioxidant, has a manila color, trapped antioxidant could have been causing the color. Also trapped solvent could have been causing the color shift since the color of the solution when the rotor was removed was a pale orange. In either case, rinsing in acetone was sufficient to remove the source of the discoloration.

B) Optical Microscopy

Viewing the fibers under cross-polars led to a number of interesting conditions. The material consisted of a large, slightly birefringent mass within which a few highly birefringent fibers could be seen, most often appearing at the fringes of the sample. Photomicrographs of typical fibers taken at a magnification of 400x are shown in Figure 17. The fibers pictured were grown at $T=91.6^{\circ}\text{C}$, stir time of 36 hours and had been washed with acetone.

The fibers shown in Figure 17 are both from the same run; however these are quite typical in appearance to those from other runs. The degree of birefringence as well as the interference color of the fibers were not uniform. The



thickness of an individual fiber varied; focusing on a section of the fibers was quite difficult. Both of the fibers shown have regions where the birefringence of the sample is very low which could be interpreted as evidence of degradation. Although not pictured, one could actually see the fibers that had been twisted; however the focusing problem made taking pictures impossible.

The fibers have diameter on the order of 10 microns and lengths of a few hundred to a few thousand microns. The length of these fibers is much less than that reported in the literature and the fibers seen here are very poorly formed. The overwhelming majority of the sample consists of the slightly birefringent amorphous material.

Differences between washed and unwashed material are seen in figures 18 and 19 respectively, magnification here is 40x. The bulk shows some crystalline material in the gelatinous layer and has a large number of fibers. It should be pointed out that this picture is not totally representative of a normal sample because the ratio of fibrous material to amorphous material is very high. The unwashed sample shows a much thicker gelatinous layer. Both samples have fibers near the fringes of the thick bulk material and also through the middle.

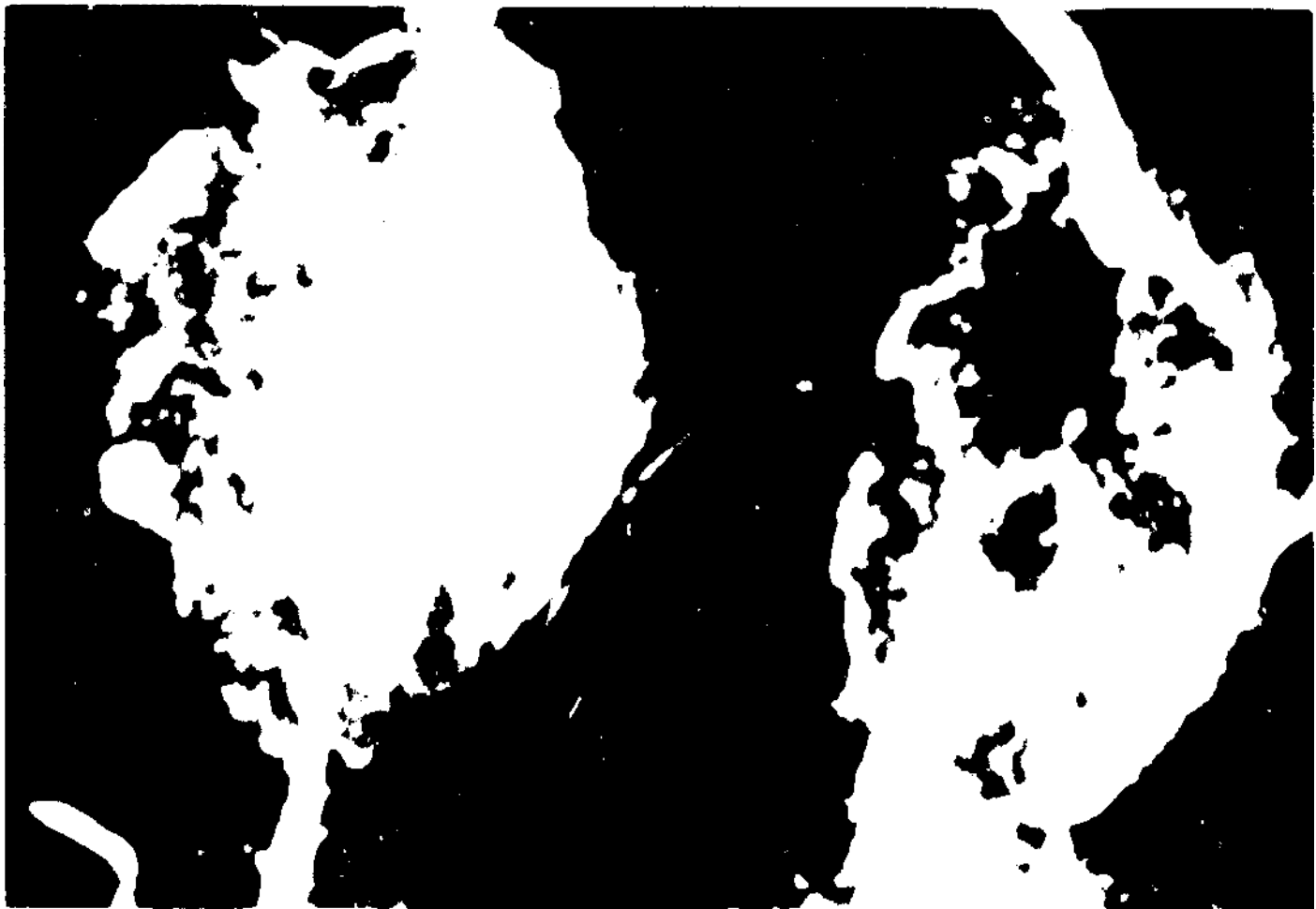


Figure 1. A person wearing a mask made of a white, textured material.

Figure 2. A person wearing a mask made of a white, textured material.



C) DSC

Porter et.al.(48) used solid state coextrusion to draw PVF₂. They successfully correlated draw ratios to the morphological forms alpha and beta. One method of characterization they used was DSC. They found that both the alpha and beta forms show a number of peaks in a DSC scan. The alpha peak was found at temperatures between 173-175° while the beta peaks occurred between 166-171°C. They also used a number of other characterization techniques, but these techniques are of no concern to this thesis.

A DSC scan of the original material (untreated polymer) is shown in Figure 20. One sees that the melting point, 159°C, is below that reported for the crystal phases of PVF₂. This reduced melting point is probably due to a large amount of crystal defects, such as a head to head or a tail to tail conformation.

A DSC scan of the unwashed fibers is shown in Figure 21 where it can be seen that the melting point is some 25°C less than the original material. This indicates the presence of a considerable amount of amorphous material and perhaps also some effects due to the molecular weight degradation referred to earlier. Trapped solvent could also cause a melting point depression. One also notes that the heat of fusion is much less for the fiber than the

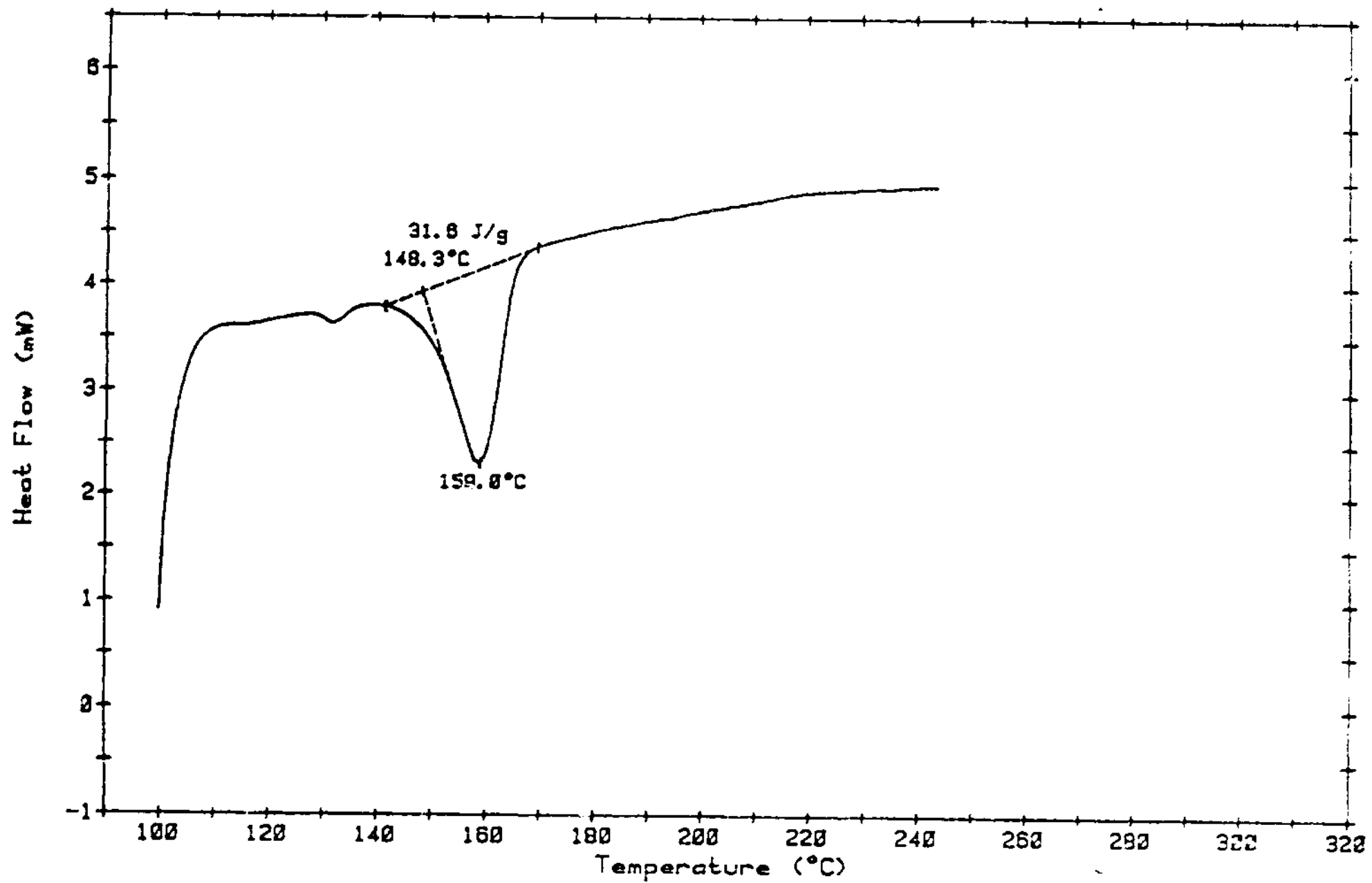


Figure 20. DSC of untreated PVF₂

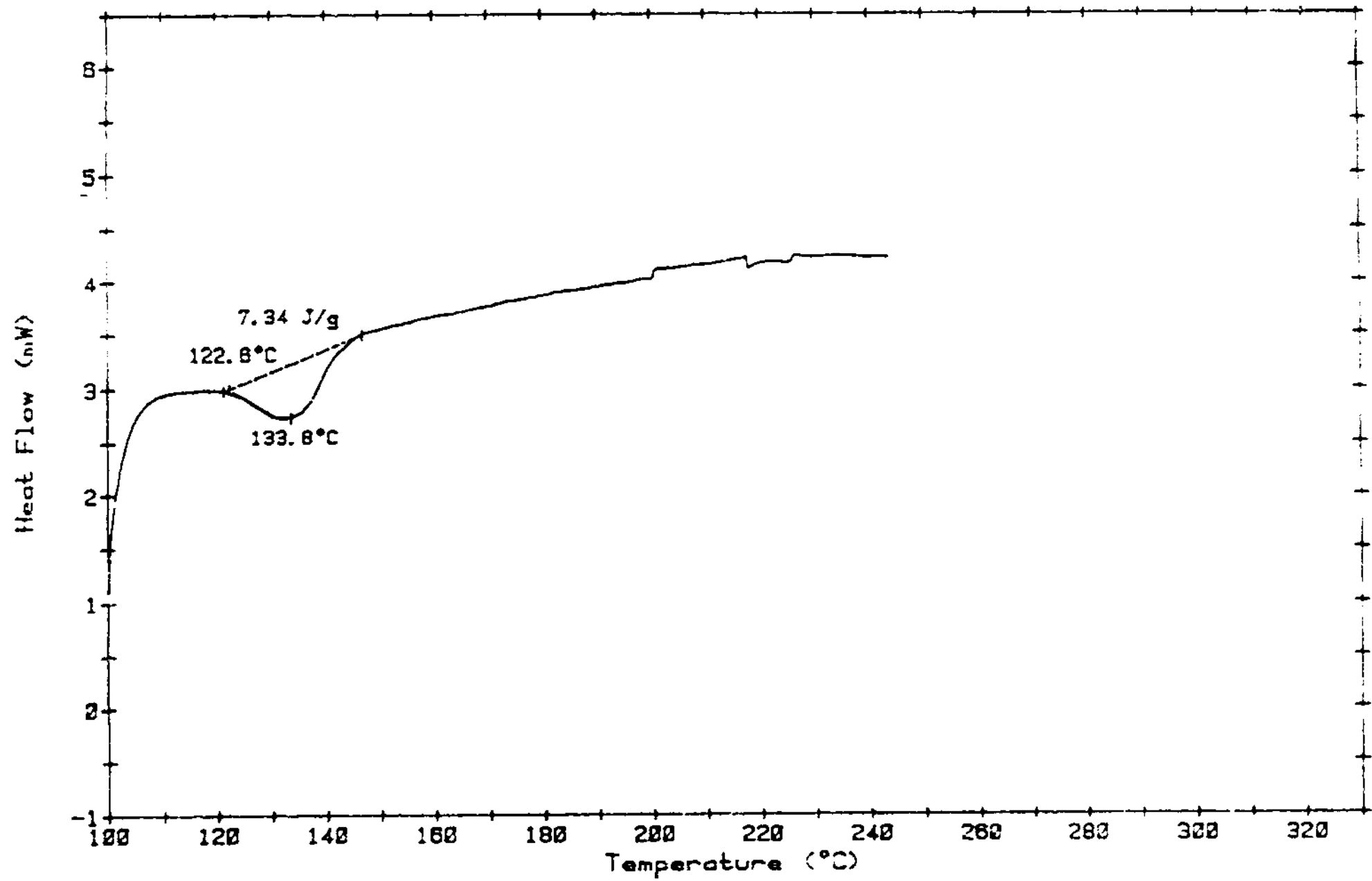


Figure 21. DSC of unwashed PVF₂ fibers

original polymer, which is again consistent with the reduced melting point.

A DSC of the washed fiber shown in Figure 22 demonstrates that the melting point is now nearly 15°C higher than the unwashed fiber; however it is still significantly less than the untreated material. This result indicates that washing the fiber dissolves some of the amorphous material, but not all, which is in agreement with the optical microscopy.

No evidence can be found on the DSC trace of a highly crystalline fiber. This absence is likely due to the very low amount of fiber present. Likewise since the baseline of the DSC trace shows drift, small peaks would be very difficult to see.

D) Shear Thickening

Two experiments were performed in DMP, one at 95°C and 0.05 wt% and the other at 104°C and 0.3 wt%. Both of the plots showed the expected shear thickening behavior; however the results could not be called conclusive.

Two techniques were developed to analyze the data. The equations necessary for data reduction are shown in the Experimental section. The two differed in the methods of calculating dt_{soln}/dt_{solv} . One fitted the data to a curve using a least squares fit and found the derivative

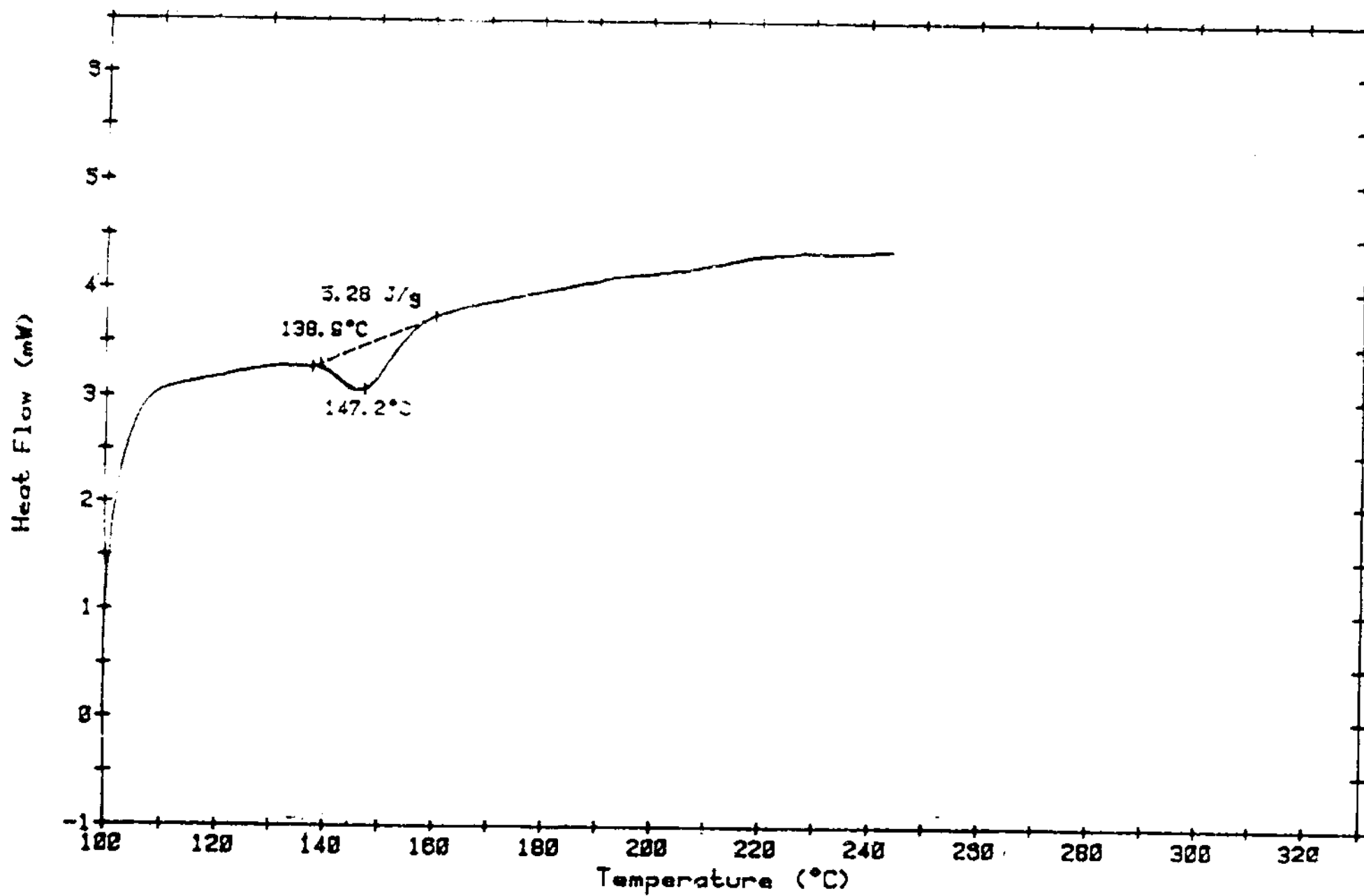


Figure 22. DSC of washed PVF₂ fibers

analytically. The other evaluated the derivative numerically. The numerical method gave plots that showed a large of scatter while the fitted curve gave relatively smooth plots.

Figures 23 and 24 show the plot of the reduced viscosity versus shear rate, figure 23 shows the plot for $T=95^{\circ}\text{C}$ and Figure 24 for $T=104^{\circ}\text{C}$. The plots do not show the expected shear thinning behavior at low shear rates, as seen in Figure 8, a feature which at present cannot be explained. All of the polymers studied by Vrahapolou (polyethylene, polypropylene and polyethylene oxide) showed the shear thinning behavior.

Shear thickening behavior is seen though, as evidenced by the maximum in the plots indicating likely entanglements, formation of which should enhance the possibility of phase separation.(26) As indicated in the background, shear thickening behavior was successfully correlated with fiber formation, i.e. only those materials that show the shear thickening behavior will form fibers. Our results therefore indicate that fibers should form.

The maximum in the reduced viscosity occurs at a much lower shear rate for the 0.3 wt% solution. The value shifts from approximately 2000s^{-1} to 1000s^{-1} . This result makes sense since entanglements should form more easily at higher concentrations. Vrahapolou found the same behavior

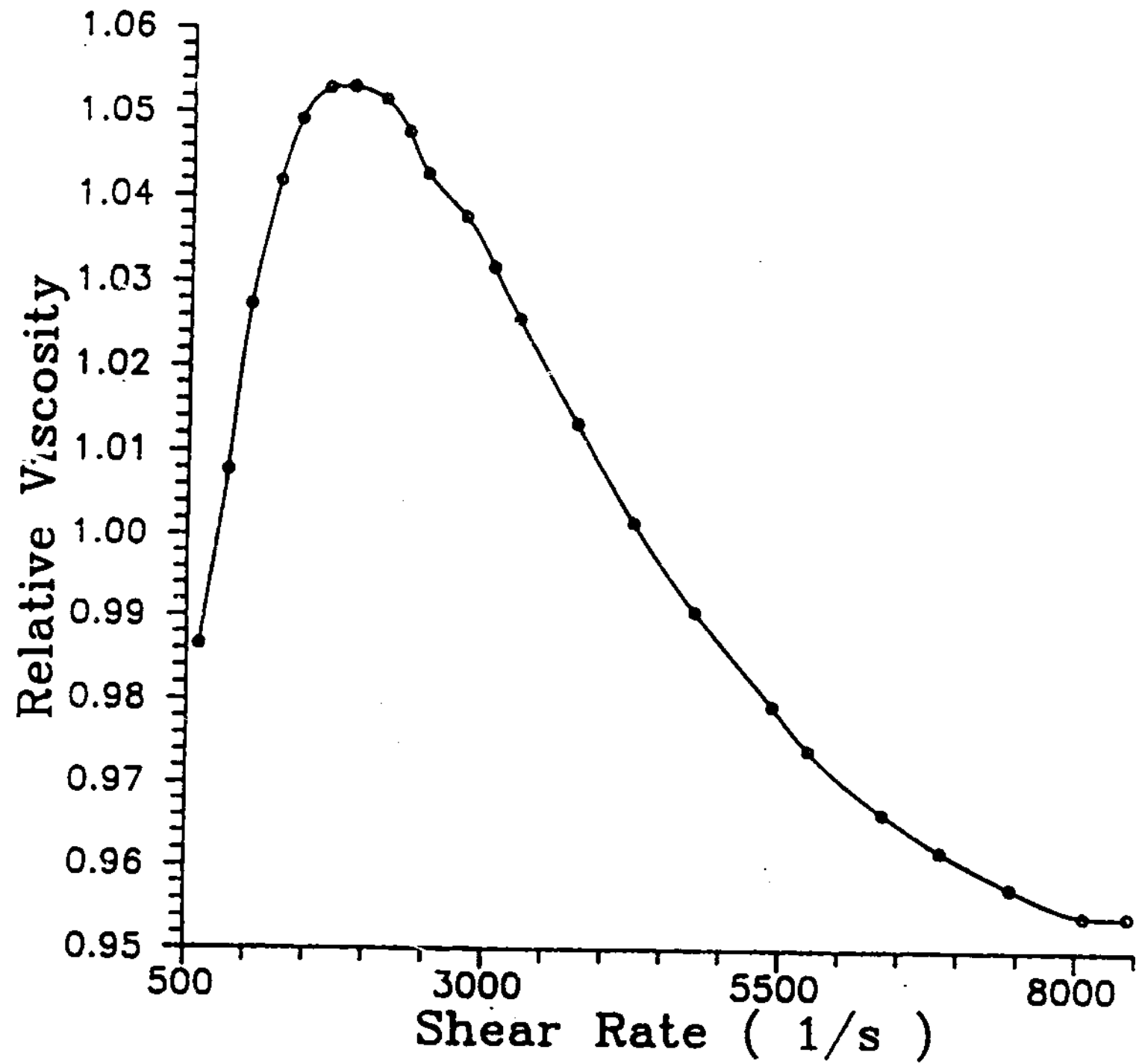


Figure 23. Plot of reduced viscosity vs. shear rate for $T=95^{\circ}\text{C}$, concentration=.05%

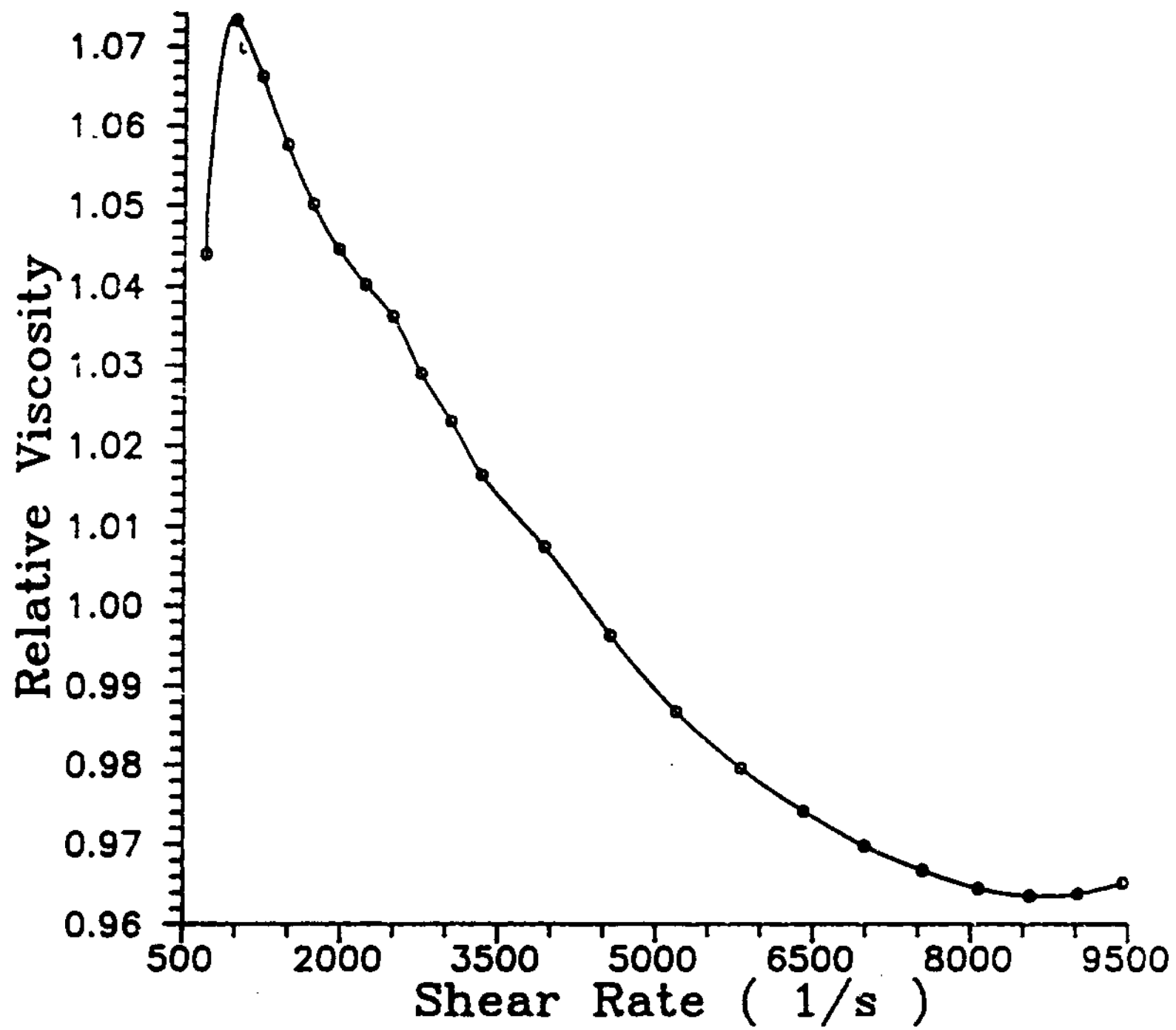


Figure 24. Plot of reduced viscosity vs. shear rate for $T=104^{\circ}\text{C}$, concentration=.34

for UHMWPE in xylene; as the concentration increased from 0.05 wt% to 0.01 wt%, the maximum in the reduced viscosity decreased from approximately $18,000\text{s}^{-1}$ to $12,000\text{s}^{-1}$.(26).

Discoloration of the solution did not occur during the experiment since the total time of a run was only 5 or 6 hours. In addition the solution made very little contact with air because nitrogen lines caused all the pressure drops.

V CONCLUSIONS AND RECOMMENDATIONS

Conclusions

1) The range of experimental conditions that produced fibers was found to be very narrow. Only one temperature, 91.6°C, one stirring rate, 350 r.p.m., and one type of rotor, teflon, consistently produced fibers.

2) Degradation is occurring, lowering the molecular weight and thus hindering the mechanism of fibrous crystallization. Degradation severely reduces the chance for flow-induced crystallization.

3) The fibers that precipitate are very poorly formed and have a large amount of amorphous material.

4) Differential Scanning Calorimetry results indicate that the precipitate fibers consist largely of amorphous material. There were however not enough crystalline fibers to influence the DSC trace.

5) Shear-thickening results indicate entanglements are forming; therefore, fibers should form.

Recommendations

- 1) The resin Soltex has a lesser amount of head to head and tail to tail defects; hence this material may produce fibers easier than Kynar and should be studied.

- 2) The fiber producing apparatus should be run under nitrogen, to determine if degradation would occur without oxygen.

- 3) The degraded solution should be tested to determine if the molecular weight of the material is actually less.

VI REFERENCES

- 1) B. Wunderlich, "Macromolecular Physics," Vol. I (1973), Vol. II (1976), Academic Press, New York.
- 2) A.J. Pennings and A.M. Kiel, Kolloid-Z.U.Z. Polymere 205, 160 (1965).
- 3) A.J. Pennings, J.V.A.A. van der Mark and H.C. Booij, Kolloid-Z.U.Z. Polymere 236, 99 (1970).
- 4) A.J. Pennings, J. Polym. Sci. Part C 16, 1799 (1967).
- 5) Z. Pelzbauer and R. St. John Manley, J. Macromol. Sci.-Phys. B(4) 4, 761 (1970).
- 6) A.C. Wikjord and R. St. John Manley, Can. J. Chem. 47, 703 (1969).
- 7) E. Kobayashi, S. Okamura and R. Signer, J. Appl. Polym. Sci. 12, 1661 (1968).
- 8) A. Keller and M.J. Machin, J. Macromol. Sci. B(1) 1, 41 (1967).
- 9) A. Lovinger in "Developments in Crystalline Polymers-1," Edited by D.C. Bassett, Applied Science Publishers (1983).
- 10) A.J. Pennings, "Proc. Int. Conf. on Crystal Growth," Boston, 389 (1966).
- 11) A.J. Pennings, J. Polym. Sci. Polym. Sym. 59, 55 (1977).
- 12) G.I. Taylor, Phil. Trans. 223A, 289 (1923).
- 13) Gieseke, Rheol. Act. 5, 239 (1966).
- 14) A.J. Pennings, H.C. Booij and J.H. Duysings, IUPAC International Symposium on Macromolecules, Leiden, 1, 263 (1970).
- 15) E.C. Frank, A. Keller and M.R. Mackley, Polymer 12, 467 (1971).

- 16) J. Rietveld and A.J. McHugh, J. Polym. Sci. Polym. Phys. Ed. 23, 239 (1985).
- 17) J. Rietveld and A.J. McHugh, J. Polym. Sci. Polym. Phys. Ed. 21, 1513 (1983).
- 18) A.J. Pennings, J. Smook, J. de Boer, S. Gogelowski and P.F. van Hutten, Pure and Appl. Chem. 55, 777 (1983).
- 19) A.J. Zwijnenburg and A.J. Pennings, Kolloid-Z.U.Z. Polymere 254, 868 (1976).
- 20) A. Coombes and A. Keller, J. Polym. Sci. Polym. Phys. Ed. 17, 1637 (1979).
- 21) J.C.M. Torfs and A.J. Pennings, J. Appl. Polym. Sci. 26, 303 (1980).
- 22) A.J. Pennings, A. Zwijnenburg and R. Lageveen, Kolloid-Z.U.Z. Polymere 251, 500 (1973).
- 23) M.R. Mackley, Kolloid-Z.U.Z. Polymere 253, 373 (1975).
- 24) J. Rietveld and A.J. McHugh, J. Polym. Sci. Polym. Phys. Ed. 23, 2359 (1985).
- 25) A. Zwijnenburg, Ph.D. Thesis, State University of Groningen, (1978).
- 26) E. Vrahapalou, Ph.D. Thesis, University of Illinois, (1986).
- 27) A.J. McHugh, Polym. Eng. and Sci. 22, 15 (1982).
- 28) A.J. Pennings in "Characterization of Macromolecular Structure," National Academy of Sciences, Washington D.C., 214 (1968).
- 29) K. Nakamura and Y. Wada, J. Polym. Sci. A-2 9, 161 (1971).
- 30) H. Kawai, Jpn. J. Appl. Phys. 8, 1975 (1969).
- 31) C. Hsu, Ph.D. Thesis, University of Illinois, (1984).
- 32) C. Mancorella and E. Martuscelli, Polymer 18, 1240 (1977).

- 33) A.J. Lovinger, J. Polym. Sci. Polym. Phys. Ed., 18, 793 (1980).
- 34) W.M. Prest Jr. and D.J. Luca, J. Appl. Phys. 46, 4136 (1975).
- 35) M. Bachmann and J. Lando, Macromolecules 14, 40 (1981).
- 36) C. Banik, P. Taylor, S. Tripathy and A. Hopfinger, Macromolecules 13, 691 (1980).
- 37) R. Hasegawa, Y. Tarahishi, Y. Chatani, H. Tadakoro, Polymer J. 3, 591 (1972).
- 38) Y. Galperin, Y. Smogalin, M. Mlenik, Vysokmol. Soed. 7, 933 (1965).
- 39) W. Doll and J. Lando, J. Macromol. Sci Phys. B2, 219 (1968).
- 40) A.J. Lovinger and H. Kerth, Macromolecules 12, 919 (1979).
- 41) Y. Galperin, B. Kosymynin and R. Bychlow, Vysokomol. Soed. B12, 555 (1970).
- 42) G. Cortilli and G. Zerbi., Spectrochim. Acta. 23A, 2216 (1967).
- 43) A.J. Lovinger, Macromolecules 13, 1317 (1980).
- 44) S. Weinhold, M. Litt and J. Lando, Macromolecules 13, 1178 (1980).
- 45) S. Weinhold, M. Bachmann, M. Litt and J. Lando, Macromolecules 15, 1631 (1982).
- 46) M. Bachmann, W. Gordon, S. Weinhold and J. Lando, J. Appl. Phys. 51, 5095 (1980).
- 47) A.J. Lovinger and D. Freed, Macromolecules 13, 989 (1980).
- 48) R. Blunk, Ph.D. Thesis, University of Illinois, (1985).
- 49) T. Shimada, A. Zachariades, W. Mead and R. Porter, J. Crystal Growth 48, 334 (1980).

50

```

real*8 slope(40), tsolv(40), tsoln(40)
real*8 Vrel(40), gamma(40)
real*8 dum1(40), dum2(40)
character*10 name
r = 0.012                                ! cm
Vbulb = 1.06                             ! ml
pi = 3.141592654
print *
print *, 'Enter data file name : '
read (5,50) name
format( 10a )
open ( unit = 10, file = name, status = 'old' )
print *
print *, 'Enter number of lines : '
read *, ndata
read (10,*)                               ! skip first line
read (10,*)                               ! skip second line
do i = 1, ndata
  read(10, *) tsolv(i), tsoln(i)
end do

close ( unit = 10, status = 'keep' )
open ( unit = 11, file = 'ans.out', status = 'new' )

print *
print *, 'Select slope calculation : '
print *, ' 1) Numerical'
print *, ' 2) Fitted'
read *, ndum
if ( ndum .eq. 1 ) then
  call deriv1( slope, tsolv, tsoln, ndata )
  write(11,*) ' Numerical Differentiation'
else
  call deriv2( slope, tsolv, tsoln, ndata )
  write(11,*) ' Fitted Curved'
endif

write(11,*) ' Shear Rate (1/s) Relative Viscosity'
write(11,*) '===== '

write(6,*) ' Shear Rate (1/s) Relative Viscosity'
write(6,*) '===== '

do i = 1, ndata
  tr = tsoln(i) / tsolv(i)
  Vrel(i) = 3.1 + slope(i) / tr
  Vrel(i) = 4.0 * tr / Vrel(i)
  gamma(i) = 4.0 * Vbulb / pi / r / r / r / Vrel(i) / tsolv(i)
  write(11,500) gamma(i), Vrel(i)
  write(6,600) tr, gamma(i), Vrel(i)
end do

500 format( f10.5, f15.1 )
600 format( f10.5, f15.1, f15.1 )

call deriv1( dum1, tsolv, tsoln, ndata )
call deriv2( dum2, tsolv, tsoln, ndata )
print *
print *, ' Brian Fitted'
write(6,*) '===== '

```

Computer Program Used for Reduction of DATA

Appendix A

```

c      do k = 1, ndata
c         print *, dum1(k), dum2(k)
c      end do
c      stop
c      end

subroutine deriv1( slope, x, y, n )
real*8 slope(40), x(40), y(40)
pi = 3.141592654
do i = 2, n - 1
c      a = sqrt( ( y(i) - y(i-1) )**2 + ( x(i) - x(i-1) )**2 )
      g = x(i+1) - x(i)
      f = y(i+1) - y(i)
      p = x(i) - x(i-1)
      q = y(i) - y(i-1)
      theta8 = atan( q / p )
      a = q / sin( theta8 )
      theta7 = atan( g / f )
      theta2 = 1.5 * pi - theta8 - theta7
      theta6 = ( pi - theta2 ) / 2.0
      phi = pi / 2.0 - theta6 - acos( q / a )
      slope(i) = tan( phi )
end do

slope(1) = slope(2)
slope(n) = slope(n-1)

return
end

subroutine deriv2 ( slope, x, y, n )
real*8 slope(40), x(40), y(40)
do i = 1, n
c      xx = x(i)
c      * soln = ( -7.63557e-3 * exp(-1.0345426*xx)
c      *      - 3.26259 * ( xx + 8.53483 )**-1.783011 ) * 1309.59
      * soln = ( -6.4934044e-3 * exp( -0.9678875*xx )
      *      - 3.52782688 * ( xx + 8.59737 )**-1.800193 ) * 1309.59
      * solv = ( -2.66120e-3 * exp(-1.0295179*xx)
      *      - 6.502243 * ( xx + 10.3245 )**-1.891819 ) * 1296.77
      slope(i) = soln / solv
end do
return
end

```